RSC Mechanochemistry

Accepted Manuscript

This article can be cited before page numbers have been issued, to do this please use: Z. T. Dowdell, P. G. Osborn, V. K. Rash, T. S. Patel, A. M. Perez, X. Lin, S. T. Holmes and R. Schurko, *RSC Mechanochem.*, 2026, DOI: 10.1039/D5MR00156K.

ROYAL SOCIETY OF CHEMISTRY

View Article Online
DOI: 10.1039/D5MR00156K

Synthesis of Organic HCl Salts via Mechanochemical Salification and their Characterization with $^{35/37}$Cl Solid-State NMR Spectroscopy

Zachary T. Dowdell[1,2], Peyton G. Osborn[1,2], Victoria K. Rash[3], Trisha S. Patel[1], Alexander M. Perez[1], Xinsong Lin[1], Sean T. Holmes[1,2,*], and Robert. W. Schurko[1,2,†]

[1] Department of Chemistry & Biochemistry, Florida State University, Tallahassee, FL 32306

[2] National High Magnetic Field Laboratory, Tallahassee, FL, 32310

[3] Department of Physics, University of Texas, Dallas, TX, 75080

[†]Deceased February 2026

*Author to whom correspondence should be addressed.

E-mail: sholmes2@fsu.edu

View Article Online
DOI: 10.1039/D5MR00156K

Abstract

Hydrochloride (HCl) salts are among the most common solid forms of active pharmaceutical ingredients (APIs) because of their favorable physicochemical properties, including enhanced solubility and stability. However, their syntheses via conventional solution-based methods are often complicated by challenges related to solvent use, stoichiometric control, phase selectivity, and environmental waste. This work presents a novel mechanochemical salification protocol that enables rapid and quantitative syntheses of a variety of organic HCl salts using precise, stoichiometric amounts of HCl. Seventeen salts were prepared from eight organic free base molecules, primarily through mechanochemistry, encompassing hydrates, anhydrous forms, and rare hemihydrochloride phases. Careful consideration is given to a variety of factors affecting these reactions, including the quantity of HCl, solvents of HCl solutions, duration and frequency of milling, the relevance of pK_a and material stability, and upward reaction scalability. Structural characterization was carried out using $^{35/37}$Cl solid-state NMR (SSNMR) spectroscopy and powder X-ray diffraction, which provide detailed insights into the local chloride ion environments and phase purities. Dispersion-corrected density functional theory (DFT-D2*) methods were used to geometry-optimize structural models based on known crystal structures and to establish correlations between $^{35/37}$Cl electric field gradient (EFG) tensors and hydrogen bonding networks essential for stabilization of crystal structures. These results demonstrate the efficiency and precision of mechanochemical salification for generating a diverse array of solid forms, as well as the utility of advanced SSNMR techniques and DFT methods for uncovering subtle structural features that govern the structures and behaviors of salts of APIs.

View Article Online
DOI: 10.1039/D5MR00156K

1. Introduction

Approximately half of the active pharmaceutical ingredients (APIs) on the market are manufactured as solid, organic HCl salts, often due to their improved physicochemical properties, such as solubility, stability, and bioavailability.[1–4] HCl salts are commonly produced via recrystallization from solution, or in some instances, by exposure to gaseous HCl[5–16]. The synthesis of HCl salts from recrystallization faces several challenges, including: (i) time-consuming evaporations; (ii) use of excessive amounts HCl and other solvents; (iii) the increased likelihood of impurity phases and/or polymorphism due to spatial heterogeneity (*i.e.*, temperature or concentration gradients); and (iv) other confounding factors that are difficult to control precisely, such as inadvertent seeding from residual solids or metastable nuclei, which can bias crystallization pathways and complicate reproducibility.[17–19]

Mechanochemistry offers better alternatives for the production of solid forms of APIs, offering advantages such as quantitative yields, minimal impurities, and short timescales (*i.e.*, minutes to hours).[20–22] Furthermore, mechanochemical reactions are often readily scalable, allowing processes developed on a small laboratory scale to be translated to large-scale industrial production.[23–28] While mechanochemical methods have been used to produce a variety of solid forms of organic molecules (*e.g.*, cocrystals, organic salts, solvates, *etc*.), there are currently no reported examples of mechanochemical synthesis of organic salts using free bases and inorganic acids (*e.g.*, HCl, HBr, H_2SO_4, *etc*.), which is surprising, given their widespread use as the preferred solid forms for many APIs. As such, *mechanochemical salification* techniques are expected to be of significant interest to academic and industrial researchers alike.

Mechanochemistry encompasses a diverse range of reaction types, with each potentially offering unique pathways for solid-state transformations. Among the most common techniques is

View Article Online
DOI: 10.1039/D5MR00156K

ball milling,[21,29] in which reagents are placed into a milling jar with ball bearings and ground at a specific frequency for a fixed duration. In many cases, a small amount of liquid is added to accelerate or enable the reaction – this is known as *liquid assisted grinding* (LAG),[30,31] whereas milling without liquid is known as *neat grinding* (NG). For larger scale reactions, mechanochemical methods such as resonant acoustic mixing, speed mixing, planetary milling, and twin-screw extrusion are increasingly employed in industrial settings to produce a variety of products, including pharmaceuticals, agrochemicals, catalysts and other advanced materials.[23,32–35] In all cases, the solvent-free or low-solvent processes enhance efficiency and sustainability, representing true instances of solid-state syntheses that adhere to the principles of green chemistry.[36,37]

The products from ball milling reactions tend to be microcrystalline powders, which hinder the use of single-crystal X-ray diffraction (SCXRD) for their characterization. However, several other analytical techniques enable their thorough characterization, including powder X-ray diffraction (PXRD), thermogravimetric analysis (TGA), IR and Raman spectroscopies, and solid-state NMR (SSNMR) spectroscopy, among others.[38–46]

Both ^{35}Cl and ^{37}Cl (spin $I = 3/2$) SSNMR are well established for characterizing HCl salts of organic molecules, including APIs, since their spectra have broad, central transition (CT, +1/2 ↔ −1/2) powder patterns that typically range from tens to hundreds of kHz in breadth, due to influences from the second-order quadrupolar interaction (SOQI) and chemical shift anisotropy (CSA).[1,47–55] The quadrupolar interaction (QI) describes the coupling between the nuclear quadrupole moment and the electric field gradient (EFG) at the nuclear origin, the latter of which is described by a symmetric, traceless, second-rank tensor. $^{35/37}$Cl EFG tensors of chloride ions in organic HCl salts are extremely sensitive to their local environments.[1,47,54–61] Since they can

View Article Online
DOI: 10.1039/D5MR00156K

easily be determined from $^{35/37}$Cl SSNMR spectra via measurement of the quadrupolar coupling constant, C_Q, and the quadrupolar asymmetry parameter, η_Q, they act as excellent probes of the complex hydrogen bonding environments of chloride ions, providing unique spectral fingerprints, permitting facile detection of impurity phases, and even enabling quadrupolar guided NMR crystallography-crystal structure prediction (QNMRX-CSP) methods for structural determination and refinement in the absence of SCXRD data.[62,63]

Despite having a larger nuclear quadrupole moment (Q) than ^{37}Cl, ^{35}Cl is typically the nucleus of choice for SSNMR experimentation due to its higher gyromagnetic ratio (γ) and higher natural abundance (n.a.). Nonetheless, ^{37}Cl SSNMR can play a complementary role due to its distinct values of γ and Q, allowing for the precise determination of the EFG and CS tensors via measurement of both ^{35}Cl and ^{37}Cl NMR spectra at a single magnetic field.[48,49,64–70] Furthermore, the $C_Q(^{35/37}\text{Cl})$ values of the chloride ions in organic HCl salts range from hundreds of kHz to *ca*. 10 MHz, meaning that $^{35/37}$Cl SSNMR spectra featuring well-defined CT patterns can be acquired with relative ease, even at lower magnetic field strengths.

Herein, we discuss efficient mechanochemical salification of eight solid free base molecules (**Scheme 1**) to produce sixteen HCl salts (eleven previously known and five newly discovered, **Table 1**), the formation of a novel salt of picolinamide produced *via* slow evaporation, and the structural characterization of all seventeen salts. We demonstrate the (i) advantages of mechanochemistry, including solid form discovery and scalability; (ii) influence of key mechanochemical parameters on reaction outcomes; (iii) relevance and limitations of solution-based synthetic principles in their application to solid-state chemical transformations; (iv) use of $^{35/37}$Cl SSNMR to investigate structure, phase identity, and sample purity; and (v) application of dispersion-corrected plane-wave DFT methods to evaluate the influence of

View Article Online
DOI: 10.1039/D5MR00156K

hydrogen-bonding networks on $^{35/37}$Cl EFG tensors, and how, in turn, they provide insight into complex, solid-state, molecular structures shaped by hydrogen bonding and other weak intermolecular interactions.

2. Experimental

2.1 Materials

Nicotinic acid (**NicA**), isonicotinic acid (**IsoA**), picolinic acid (**PicA**), acetaminophen (**Acet**), nicotinamide (**Nic**), isonicotinamide (**Iso**), picolinamide (**Pic**), and caffeine (**Caff**) (**Scheme 1**) were purchased from MilliporeSigma and used without further purification. These reagents were used to mechanochemically synthesize eleven previously-reported salts, including: nicotinamide hemihydrochloride hydrate (**NicH-Nic:H_2O**), nicotinamide HCl (**NicH**), isonicotinamide HCl (**IsoH**), nicotinic acid HCl **(NicAH**), isonicotinic acid HCl (**IsoAH**), picolinic acid HCl monohydrate (**PicAH:H_2O**), anhydrous picolinic acid HCl (**PicAH**), caffeine HCl dihydrate (**CaffH:H_2O**), caffeine HCl (**CaffH**), bis(acetaminophen) HCl (**AcetH-Acet**), and acetaminophen HCl monohydrate (**AcetH:H_2O**).[7–15] In addition, they were also used to produce six novel salts, including: isonicotinamide-isonicotinamidium chloride monohydrate (**Iso-IsoH:H_2O**), picolinamide HCl monohydrate (**PicH:H_2O**), picolinamide HCl (**PicH**), picolinamide-picolinamidium chloride (**PicH-Pic**), picolinic acid hemihydrochloride (**PicAH-PicA**), and (bis)acetaminophen HCl monohydrate (**Acet-AcetH:H_2O**).

View Article Online
DOI: 10.1039/D5MR00156K

2.2 Synthesis of HCl Salts

HCl salts were synthesized using slow evaporation and/or mechanochemical grinding. Mechanochemical syntheses were carried out under a variety of conditions using 12.1 M HCl(aq), 3.0 M methanolic HCl (HCl(MeOH)), or 1.25 M ethanolic HCl (HCl(EtOH)) as milling liquids. Ball milling reactions used 10 mL Teflon milling jars with one 10 mm Teflon ball bearing and were conducted using a Retsch Mixer Mill 500 Vario with a milling frequency ranging from 20 to 35 Hz, and milling times ranging from 2 to 15 min (unless specified otherwise). For larger scale reactions conducted with 75 or 100 g of solids, a FlackTek Model 330-100 SE speed mixer was used with 250 mL polypropylene sample holders at 2000 RPM for 2 minutes. The optimized milling conditions for efficient, high-yield, lab-scale syntheses are presented in **Table 1**. No further grinding of reaction products was needed prior to analyses by SSNMR or PXRD. For syntheses *via* slow evaporation, a solution containing one organic reagent was dissolved in a 20 mL glass vial with gentle heating at *ca.* 55 °C to completely dissolve the solids. The solutions were allowed to evaporate for several days to weeks under ambient conditions. Suitable crystals were used for analysis by SCXRD.

2.3 Powder X-ray Diffraction

PXRD patterns were acquired on a Rigaku Miniflex with a Cu *K*α (λ = 1.540593 Å) radiation source and a HyPix-400 MF 2D hybrid pixel array detector. The X-ray tube voltage and amperage were set to 40 kV and 15 mA, respectively. Experiments were run with the detector scanning 2θ angles from 2.5° to 50° with a step size of 0.03° at a speed of 5° min^{-1}. The PXRD patterns for all reagents and cocrystals were compared to patterns simulated from reported

View Article Online
DOI: 10.1039/D5MR00156K

structural models[7–15,71–80] using the CrystalDiffract[81] software package to confirm crystallinity and purity, and to identify novel phases (**Figs. S1 – S7**).[81]

2.4 Single-Crystal X-ray Diffraction

A clear light yellow, irregular shaped crystal of **PicH:H_2O** was mounted on a nylon loop with perfluoroether oil. The sample was crystallized by a diffusion method. Data were collected from a shock-cooled single crystal at room temperature on a XtaLAB Synergy, Dualflex, HyPix four-circle diffractometer with a micro-focus sealed X-ray tube using a mirror as monochromator and a HyPix detector. The diffractometer was equipped with an Oxford Cryostream 800 low-temperature device and used Cu *K*α radiation (λ = 1.54184 Å). All data were integrated with Crysalispro and a gaussian absorption correction using SCALE3 ABSPACK was applied. The structure was solved by dual methods using SHELXT[82] and refined by full-matrix least-squares methods against F^2 by SHELXL.[83] All non-hydrogen atoms were refined with anisotropic displacement parameters. All C-bound hydrogen atoms were refined isotropic on calculated positions using a riding model with their U_{iso} values constrained to 1.5 times the U_{eq} of their pivot atoms for terminal sp^3 carbon atoms and 1.2 times for all other carbon atoms. Disordered moieties were refined using bond lengths restraints and displacement parameter restraints. Crystallographic data for the structure reported in this paper has been deposited with the Cambridge Crystallographic Data Centre under the deposition number 2341820.

2.5 Thermogravimetric Analysis

Thermogravimetric analysis (TGA) measurements were performed on a TA Instruments TGA 550 with samples packed in alumina crucibles. Samples were heated from room

View Article Online
DOI: 10.1039/D5MR00156K

temperature (~23°C) to 400°C at a heating rate of 10 °C min^{-1} under a dry argon purge (gas flow of 25 ml min^{-1}).

2.6 Solid-State NMR Spectroscopy

2.6.1 Overview. SSNMR experiments were conducted at the National High Magnetic Field Laboratory (NHMFL) in Tallahassee, FL. Experiments at B_0 = 18.8 T [$\nu_0(^1H)$ = 800.13 MHz, $\nu_0(^{35}Cl)$ = 78.42 MHz, and $\nu_0(^{37}Cl)$ = 65.35 MHz] were conducted on Bruker Avance NEO spectrometer with an Oxford standard bore magnet. Magic-angle spinning (MAS) and static (stationary sample) experiments were carried out with NHMFL-built 5.0 mm HX or 3.2 mm HXY probes, with samples packed into 3.2 zirconia oxide rotors (^{35}Cl static/MAS) or 5.0 mm o.d. polychlorotrifluoroethylene sample holders (^{37}Cl static).

2.6.2 $^{35/37}$Cl SSNMR. Static $^{35}Cl\{^1H\}$ SSNMR spectra were obtained at 18.8 T using a variety of pulse sequences (Hahn Echo,[84] QCPMG,[85–87] CP-CPMG,[88–90] and WURST-CPMG[91–93]) with a continuous wave (CW) ^1H decoupling field of 50 kHz. All WURST pulses used a 500 kHz sweep width. $^{37}Cl\{^1H\}$ static spectra were obtained using Hahn Echo, QCPMG, or CP-CPMG pulse sequences, with CW ^1H decoupling field of 50 kHz. $^{35}Cl\{^1H\}$ MAS spectra were obtained using a Bloch decay or rotor-synchronized Hahn Echo or QCPMG pulse sequence, with an MAS rate of ν_{rot} = 10 - 20 kHz and 50 kHz of SPINAL-64 deocupling.[94–96] $^{35/37}Cl$ chemical shifts were referenced to 1.0 M NaCl(aq) (δ_{iso} = 0.0 ppm) using NaCl(s) (δ_{iso} = −41.1 ppm) as a secondary reference. Experimental details are provided in **Tables S1 – S2**. Pulse sequences and recommended calibration parameters and standards are available from the authors by request or at https://github.com/rschurko.

View Article Online
DOI: 10.1039/D5MR00156K

2.6.3 Spectral Processing and Simulation. Spectra were processed using the TopSpin v.3.7 software package. Simulations of $^{35/37}$Cl SSNMR spectra were generated using the ssNake v.1.5 software package.[97] Euler angles extracted from simulations in ssNake, which use the *ZX′Z″* convention, were converted to the *ZY′Z″* convention and verified through additional simulations in WSolids1.[98,99]

2.7 DFT Calculations

Calculations were performed on structural models based on previous SCXRD studies,[7–15,71,100] with the exception of **PicH:H$_2$O**, for which the structural model is based on the SCXRD structure reported herein. Geometry optimizations and subsequent calculations of ^{35}Cl EFG and magnetic shielding tensors were performed using dispersion-corrected plane-wave DFT methods (DFT-D2*)[101,102] using the CASTEP module[103,104] within Materials Studio 2020. These calculations used the generalized gradient approximation (GGA) with the RPBE functional,[105] ultrasoft pseudopotentials generated on-the-fly,[106] a *k*-point spacing of 0.05 Å^{-1}, a plane-wave cut-off energy of 800 eV, and an SCF convergence threshold of 5×10^{-7} eV. Geometry optimizations employed the LBFGS method,[107] in which the positions of all atoms were relaxed with unit cell parameters fixed at their experimental values. Thresholds for structural convergence included a maximum change in energy of 5×10^{-6} eV atom^{-1}, a maximum displacement of 5×10^{-4} Å atom^{-1}, and a maximum Cartesian force of 10^{-2} eV Å^{-1}. A correction to the dispersion energy was introduced using Grimme's semi-empirical two-body dispersion force field,[108,109] with an empirical reparameterization introduced by our group.[101,102,110] ^{35}Cl magnetic shielding tensors were calculated using the GIPAW method.[111] ^{35}Cl chemical shift values were referenced with respect to that of NaCl(s) (δ_{iso} = −41.1 ppm), which has an absolute

View Article Online
DOI: 10.1039/D5MR00156K

isotropic magnetic shielding value of 993.28 ppm. EFGShield[112] was used to extract the Euler angles describing the relative orientations of magnetic shielding and EFG tensors, which are reported using the *ZY′Z″* convention for rotation.[99]

3. Results and Discussion

3.1 Overview

In this section, we discuss: (i) the mechanochemical syntheses of previously reported and novel organic HCl salts; (ii) considerations for their optimized mechanochemical syntheses; (iii) their characterization using SSNMR, XRD, and TGA; and (iv) DFT-D2* calculations for refinement of crystal structures and prediction of $^{35/37}$Cl EFG tensors. $^{35/37}$Cl SSNMR is highlighted as the key characterization method due to the unique $^{35/37}$Cl CT powder patterns resulting from the diverse hydrogen bonding arrangements of the chloride ions in organic HCl salts. DFT calculations are used to correlate the ^{35}Cl EFG tensors to the local hydrogen bonding environments of the chloride ions, which is crucial for understanding their roles in stabilizing their solid-state structures.

The outcomes of all mechanochemical syntheses were assessed using PXRD data, with patterns acquired for all previously reported and novel organic HCl salts (**Figs. S1** - **S7**). Those of the former are in good agreement with simulated patterns based on their crystal structures, while those of the latter are compared to patterns of educts, with distinct diffraction peaks attributed to novel phases (based on this, the stoichiometry of the reaction, and no detection of impurities via PXRD and/or other analytical techniques, *vide infra*). The PXRD pattern of **PicH:H$_2$O** was also compared to simulated patterns derived from the novel crystal structure

View Article Online
DOI: 10.1039/D5MR00156K

reported herein and found to be in agreement. These results confirm that the syntheses are successful, and the products are crystalline with no presence of impurities.

3.2 Mechanochemical Salification Methods for the Synthesis of Organic HCl Salts

Eleven known and five novel organic HCl salts were synthesized in essentially quantitative yields and high purities via mechanochemical salification, and one novel organic HCl salt was produced via slow evaporation, as evidenced by PXRD (referred to throughout **§3.2**) and ^{35}Cl SSNMR (see **§3.6.3**). Optimized LAG conditions and ball milling parameters are reported in **Table 1**. Generally, the role of ball milling appears to be that of mixing of reagents, consistent with the acid-base neutralization reactions that often occur spontaneously for such systems. However, there are many factors that play a role in the formation of the desired salt with minimal impurities and waste, as discussed in the text that follows.

3.2.1 Impact of the Quantity of HCl. In most solution-based salification reactions, HCl is added in significant excess (*e.g.,* fully dissolving a solid free base in concentrated HCl);[7,8] however, with mechanochemical methods, it is possible to use microliters of solvent in precise molar ratios to target specific products. Generally, if multiple solid phases differ in their chloride content, the relative stoichiometry of HCl governs which phase is obtained. For example, **NicH-Nic:H_2O** and **NicH** were both synthesized *via* LAG using precise stoichiometric amounts of 12.1 M HCl(aq) to target the desired product (*i.e.*, half an equivalent was used for **NicH-Nic:H_2O**, whereas one equivalent was used for **NicH**). If more than half an equivalent of HCl is added, the formation of **NicH** is favored due to preferred protonation of the pyridyl nitrogen. A slight excess of acid can also facilitate the synthesis of a specific product by preventing side reactions or driving the reaction forward in cases where optimizing other synthetic parameters is

View Article Online
DOI: 10.1039/D5MR00156K

unfeasible (*e.g.*, in the salification reactions that yield **AcetH:H_2O** and **PicAH**, two equivalents of HCl is used to eliminate impurities and/or unreacted educts).

3.2.2 Impact of the Solvent of HCl Solutions. The choice of solvent can have a considerable impact on mechanochemical reactions.[31,113–115] Herein, three distinct solvents were used for concentrated HCl solutions, including 12.1 M HCl(aq), 3.0 M methanolic HCl (HCl(MeOH)) and 1.25 M ethanolic HCl (HCl(EtOH)). In the cases of **PicA**, **Caff**, and **Acet**, the solvent determines which salt is formed. Use of HCl(aq) leads to the production of the hydrates **PicAH:H_2O**, **CaffH:H_2O**, and **AcetH:H_2O**, whereas use of HCl(MeOH) or HCl(EtOH) leads to the formation of the anhydrous salts **PicAH**, **CaffH**, and **AcetH**. This contrasts with the case of **NicA**, where the solvent is relatively unimportant, as **NicAH** appears to be the only possible product (*i.e.*, no hydrate or solvate phases have been observed in our reaction product mixtures). The use of different HCl solvents also offers insights into the nature of the products. For example, **PicAH-PicA** was determined to be anhydrous due to the identical products obtained from reactions involving either HCl(aq) and HCl(MeOH). Similarly, **IsoH-Iso:H_2O** was determined to be a hydrate, since use of half an equivalent of HCl(MeOH) produced a mixture of **IsoH** and unreacted **Iso**.

Hence, altering both the amount of HCl and its solvent offers additional pathways for synthesizing novel materials. In certain cases, different HCl solvents may result in different reaction mechanisms that either lead to the same product, or perhaps a distinct polymorph or solvate.[25,31,55,116–119] As such, it is possible that other systems may exhibit even more complex behavior. However, use of HCl(aq) is generally preferred, since its high HCl concentration is associated with significantly less solvent in comparison to concentrated alcoholic HCl (*e.g.*, in the preparation of 100 mg of **NicH**, 70 μL of HCl(aq) is necessary, which corresponds to *ca*. 300

View Article Online
DOI: 10.1039/D5MR00156K

μL of HCl(MeOH) or 700 μL of HCl(EtOH)). However, methanol and ethanol are more easily evaporated than water, given that they are *ca*. five and two times as volatile under standard temperature and pressure (this is based on calculations using the Clausius-Clapeyron equation, assuming boiling points of 64.7, 78.4, and 100.0 °C for MeOH, EtOH, and H_2O, respectively).

3.2.3 Impact of Milling Duration and Milling Frequency. Two important considerations for almost all ball milling reactions are the milling duration and milling frequency. Generally, a sufficient milling duration is required to drive the reaction to completion and ensure formation of the desired products, whereas the milling frequency impacts the rate of the reaction. In most of the cases presented herein, milling at 20 Hz for 5 to 15 minutes is sufficient for the formation of an HCl salt with no trace of educts (*i.e.*, unreacted free bases) or other impurities. However, as the milling duration or milling frequency increases, the temperature inside the milling jar increases as well, which may impact the reaction and end products.[120]

Heating hydrates of organic HCl salts sometimes results in the release of water, leading to an anhydrous solid. For example, excess heating of **CaffH:H_2O** causes dehydration and disproportionation to **Caff**, releasing H_2O and HCl.[121] This effect can be replicated in LAG reactions intended for the production of **CaffH:H_2O**, where milling at a higher frequencies and/or longer durations results in the presence of **Caff** impurities.

The synthetic pathways for the various HCl salts of **PicA** (**Fig. 1**) highlight the heat-dependent transformation of **PicAH-H_2O** to **PicAH-PicA**. If the desired product is **PicAH:H_2O**, the formation of **PicAH-PicA** needs to be prevented. There are several options to accomplish this, all of which can be used in tandem: (i) addition of excess HCl(aq) causes any **PicAH-PicA** that is formed to convert to **PicAH:H_2O**; (ii) use of cryogens can be employed to avert the

View Article Online
DOI: 10.1039/D5MR00156K

buildup of heat, preventing the formation of **PicAH-PicA**; and (iii) reducing the milling time and/or frequency can be used to decrease the time the material is exposed to heat and/or reduce the rate of heat generation. Other parameters also impact the maximum temperature reached, such as the materials of the jar and ball bearings, as well as the amount of material being milled. These are very important considerations for scaling up the reaction size for industrial production.[120]

3.2.4 Impact of pK_a and Material Stability – An Investigation Using Competitive Milling. The protonation behavior of the molecules in **Scheme 1** is strongly influenced by their functional groups and positions on the pyridyl ring. Amide groups, such as those in **Nic**, **Iso**, and **Pic**, act as weak electron-withdrawing substituents, which decreases the basicity of the pyridyl nitrogen and makes protonation less favorable in comparison to an unsubstituted pyridyl ring (*e.g.*, pK_a's of the pyridyl nitrogen are 3.4 and 5.2 for **Nic** and pyridine, respectively). Similarly, carboxylic acid moieties, such as those in **NicA**, **IsoA**, and **PicA**, serve as stronger electron-withdrawing groups, further reducing the basicity of the pyridyl nitrogen and making protonation even less favorable. The position of the substituent relative to the pyridyl nitrogen also plays a key role in modulating electronic effects. Electron-withdrawing groups positioned closer to the pyridyl nitrogen exert a stronger inductive effect, as in the case of **Pic**, where electron density is withdrawn more effectively from the pyridyl nitrogen than in **Nic** or **Iso**. Furthermore, substituents in the *ortho* and *para* positions engage in resonance with the pyridyl ring, resulting in a greater reduction in basicity than would be predicted from inductive effects alone.

To investigate the impact of these effects in the context of mechanochemical salification, we conducted a series of competitive milling reactions (**Table 2**).[122,123] An equimolar amount of two free bases (*e.g.*, **Nic** and **NicA**) were added to a milling jar with either one or half a molar

View Article Online
DOI: 10.1039/D5MR00156K

equivalent of HCl(aq), and ball milled. The product was then characterized to determine which phase(s) of material is(are) formed. The pK_a values for the six starting materials are in **Table S3**[124] and the PXRD patterns for the reaction products are given in **Figs. S8-S18**.

The enthalpies of formation (ΔH_f, **Table S4**) were derived from the equation:

$$\Delta H_f = H_{product} - (AH_{educt}^{(1)} + BH_{educt}^{(2)} + CH_{water}) \quad \textbf{(1)}$$

where $H_{product}$, H_{educt}, and H_{water} correspond to the DFT-derived static lattice energies of the products, educts, and water, respectively, and the coefficients A, B, and C correspond to the stoichiometric amounts of each educt and water, where H_{water} is only considered for hydrates. While many of the values of ΔH_f are only slightly negative or even positive, there are several possible explanations for why the reaction still proceeds: (i) some portion of the solid is dissolved, which is not captured in static lattice energy models;[21] (ii) the reaction may be driven through product precipitation, which shifts the equilibrium irreversibly forward;[31] (iii) there are relatively large errors in these calculated values as finite temperature effects are not taken into account;[125–127] and (iv) mechanochemical effects, such as defect formation and local heating, contribute additional energy to drive the reaction forward.[128,129]

First, the competitive milling reactions of mixtures of amides and carboxylic acids with HCl are considered. For **Nic**, **NicA**, **Iso**, and **IsoA**, the reactions proceed as expected, where the more basic **Nic** and **Iso** molecules are protonated instead of **NicA** and **IsoA** (*i.e.*, only **NicH** and **IsoH** are formed, perhaps due to the higher pK_a's of their pyridyl nitrogens). However, similar reactions with **Pic** and **PicA** yield the salt **PicAH-PicA**, as well as a picolinamide picolinic acid cocrystal (**Pic-PicA**),[130] meaning that **Pic** reacts with the weak acid **PicA,** rather than the significantly stronger HCl. Without a crystal structure for **Pic-PicA**, it is difficult to say whether

View Article Online
DOI: 10.1039/D5MR00156K

this is a result of a kinetically-favored reaction or if the cocrystal is more thermodynamically stable than **PicH**, **PicH:H_2O**, **PicAH**, and/or **PicAH:H_2O**.

Second, reactions of mixtures of amides with HCl are discussed. Both the 1:1:1 and 1:1:0.5 reactions of **Nic**, **Iso**, and HCl yield a nicotinamide-isonicotinamide cocrystal (**Nic-Iso**).[130] This is interesting, as the ΔH_f for **Nic-Iso** is significantly higher than that of **NicH** or **IsoH**, meaning a less thermodynamically favorable product is formed. We observe the salt **IsoH-Iso:H_2O** and excess **Nic** in the 1:1:1 case, suggesting that excess acid is needed to drive the reaction forward. Similarly, reactions of **Nic**, **Pic**, and HCl yield **NicH-Nic:H_2O** as well as a nicotinamide-picolinamide cocrystal (**Nic-Pic**),[130] further highlighting the possibility of kinetically driven reactions. We also note that **NicH-Nic:H_2O** is formed in the 1:1:1 reaction, suggesting that **Nic-Pic** formation competes poorly under these conditions in comparison to **Nic-Iso** and **Pic-PicA**. The reactions of **Iso**, **Pic**, and HCl result in the production of an unknown solid form, which is suspected to be an ionic cocrystal of **Iso**, **Pic**, and HCl (**Iso-Pic:HCl**) as evidenced by a unique ^{35}Cl SSNMR spectrum (see **§3.6.3**, **Fig. S19**), but this is not explored further in this work. However, since there is PXRD evidence of unreacted **Pic** in the final reaction mixture, it is likely that this cocrystal does not have a 1:1:1 stoichiometric ratio of the three components.

Finally, the reactions of mixtures of carboxylic acids with HCl are explored. **NicA**, **IsoA**, and HCl react in a 1:1:1 ratio to form **NicAH** and **IsoA**; however, some **IsoAH** is also observed, whereas the 1:1:0.5 reaction yields **NicAH** as the only salt, with excess **IsoA** and **NicA**. However, the 1:1:1 **NicA** + **PicA** + HCl reaction yields **NicAH**, **PicAH:H_2O**, and educts, whereas the 1:1:0.5 reaction yields **PicAH-PicA**, **PicAH:H_2O**, and residual **NicA**. Both reaction ratios for **IsoA**, **PicA**, and HCl yield **PicAH:H_2O** as the only salt (plus residual **IsoA**).

View Article Online
DOI: 10.1039/D5MR00156K

In these competitive milling reactions, neither the pyridyl nitrogen basicity (as predicted by pK_a) nor thermal stabilities are the sole predictors of the products. Even the assumption that one of these educts would react with HCl is sometimes incorrect, as seen by the formation of the **Pic-PicA**, **Nic-Iso**, and **Nic-Pic** cocrystals. In mechanochemical reactions, there are additional factors to consider. First, there are clear limitations of using pK_a values to predict the outcomes of solid-state reactions, since they are derived from solution measurements, and do not account for the array of additional solid-state interactions, including intermolecular hydrogen bonding and molecular packing that influence intrinsic basicity/acidity. Second, since mechanochemical reactions involving organic compounds are thought to initiate on the surfaces of particles that are being ground or sheared together,[131–133] it is possible that some reactions are kinetically driven, which may supplant simple considerations of acidity, basicity, and/or thermodynamics. While we are unable to provide a succinct and satisfying explanation for these phenomena, it is clear that predictions based on simple solution-phase principles do not apply to mechanochemical reactions; nonetheless, this opens a wider canvas for exploration of the production of HCl salts and related cocrystals.

3.3 Mechanochemical Screening of Novel Phases of Hemihydrochloride Salts

High-throughput recrystallizations are often preferred for screening due to the relative ease of setting up many reactions under a variety of synthetic conditions.[134,135] However, mechanochemistry may have an edge in discovering more unusual phases in situations where the stoichiometric ratio of the organic free base (FB) to the number of chloride ions is greater than 1:1, such as in the case of hemihydrochloride salts (*e.g.*, FB:HCl = 1:0.5, like in the cases of **IsoH-Iso:H_2O**, **PicAH-PicA**, *etc*.). For example, **NicH-Nic:H_2O** was first synthesized via a two-

View Article Online
DOI: 10.1039/D5MR00156K

step slow evaporation over the course of several weeks.[71] However, we report its quantitative synthesis in as little as 2 min, with no detectable byproducts or impurities. The ability to target specific molar ratios with HCl in various solvents allows for facile screening using mechanochemical methods and the exploration of novel solid forms.

3.4 Syntheses of Novel HCl Salts

Here, we discuss the mechanochemical syntheses of five novel materials: **IsoH-Iso:H_2O**, **PicH-Pic**, **PicH**, **PicAH-PicA**, **AcetH-Acet:H_2O**, along with the formation of **PicH:H_2O** via slow evaporation (reaction summaries are again given in **Table 1**). The hemihydrochloride salts (*i.e.*, **IsoH-Iso:H_2O**, **PicH-Pic**, **PicAH-PicA**) were synthesized with ratios of 1:0.5 FB:HCl. We also attempted to prepare these materials with 12.1 M HCl(aq) or 3.0 M HCl(MeOH) to confirm their hydration states, finding that either solvent led to the formation of **PicH-Pic** and **PicAH-PicA**, whereas only HCl(aq) led to **IsoH-Iso:H_2O**. **PicH** can be formed with a 1:1 ratio of FB:HCl with either HCl(EtOH) or HCl(MeOH), suggesting that it is anhydrous. Ball milling **Acet** and 12.1 M HCl(aq) in a 1:1 molar ratio yields what we suspect to be **AcetH-Acet:H_2O**, since a 1:2 ratio yields **AcetH:H_2O** and a 1:0.5 ratio yields a mixture of **Acet** and **AcetH-Acet:H_2O** (**Fig. S20**). Due to the relatively poor basicity of the secondary amide, it is unclear whether **AcetH-Acet:H_2O** is a hemihydrochloride requiring optimized milling conditions, if it is a polymorph of **AcetH:H_2O**, or if it exists in a unique, non-standard molar ratio. While mechanochemical methods alone cannot give a definitive answer on the nature of this material, TGA can (see **§3.6.1)**.

The synthesis of **PicH:H_2O** is unique in this work, being non-mechanochemical. Two equivalents of HCl(aq) are enough to fully dissolve **Pic** while milling, with subsequent

View Article Online
DOI: 10.1039/D5MR00156K

evaporation of excess solvent leading to the formation of **PicH:H_2O**. The formation of this material is likely better suited for slow evaporation, as straightforward milling of **PicH** with different molar equivalents of H_2O does not lead to the formation of **PicH:H_2O**. This slow evaporation synthesis yielded crystals suitable for SCXRD structure determination (see **§3.6.1**).

3.5 Mechanochemical Scale-Up

The mechanochemical salification methods outlined herein have the potential to be used on an industrial scale. To explore this, a speed mixer was used with larger quantities of free base solids and 12.1 M HCl(aq) to produce **NicH**, **NicH-Nic:H_2O**, **NicAH**, and **CaffH** in amounts between 75 and 100 g in quantitative yields (*i.e.*, no detectable educts or impurities in the PXRD patterns, **Fig. S21**) in as little as 2 minutes at 2000 RPM (**Table 3**, first four rows). This was accomplished using the same reaction chemistries listed in **Table 1**, with near stoichiometric amounts of HCl and no ball bearings. Further reactions to even larger scales were not attempted due to weight limitations of the speed mixer in our laboratory; however, this shows promise for scaling such reactions into the kilogram regime with the appropriate equipment. As these salification reactions are exothermic (*i.e.*, reaction vessels became warm to the touch), thermal effects should be considered during further scale-up, particularly when working with concentrated HCl and larger batch masses under confined mixing conditions. Again, of particular note are the high yields, minimal impurities, low solvent use, and reduced time scales compared to solvent-based recrystallizations. These reactions also maintain low process mass intensities (PMIs) at larger scales (**Table 3**), reflecting the near-stoichiometric use of HCl and minimal liquid loading relative to conventional hydrochloride salt crystallization methods.

View Article Online
DOI: 10.1039/D5MR00156K

3.6 Structural Characterization of Organic HCl Salts

3.6.1 Single-crystal X-ray Diffraction. Slow evaporations were attempted for all novel materials in hopes of obtaining crystals suitable for analysis by SCXRD; however, only recrystallizations of **PicH:H_2O** were successful. **PicH:H_2O** crystallizes in the monoclinic space group $P2_1/n$ featuring a single chloride ion site (**Fig. 2**). This crystal structure is available from the Cambridge Structural Database under deposition number 2341820.

3.6.2 Thermal Analysis. TGA was used to characterize the novel hemihydrochloride salts **IsoH-Iso:H_2O**, **PicH-Pic**, **PicAH-PicA**, and **AcetH-Acet:H_2O**, with the goal of determining their hydration state. First, since the molar mass of **IsoH-Iso:H_2O** is 298.73 g mol^{-1}, *ca*. 6% of its mass is attributed to water. This is confirmed by a *ca*. 7% mass reduction over a temperature range from 35 to 145 °C (thermal degradation occurs at *ca*. 155 °C, **Fig. S22**). The additional *ca*. 1% loss may arise from moisture content in the sample. Second, the TGA results for **PicH-Pic** and **PicAH-PicA** are inconclusive due to the inherent thermal instability of their components. **PicAH** thermally degrades at temperatures as low as 55.2 °C, and **Pic** has an even lower melting point than **PicA** (*i.e.*, 110 °C vs. 136 °C), making both materials poor candidates for thermal analysis.[136] Consistent with this, thermal degradation for **PicH-Pic** and **PicAH-PicA** begins near 80 °C (**Figs. S23** and **S24**). Prior to this, there is a small mass reduction of *ca*. 5%, which could arise from either the partial release of waters of hydration, resulting in a smaller than expected weight loss for a monohydrate, or the presence of "surface" water molecules (*i.e.*, physisorbed, chemisorbed, and/or interstitial water molecules that are not part of the crystalline lattice). However, as described in **§3.4**, these materials can be synthesized under anhydrous conditions, making the presence of waters of hydration unlikely. Finally, **AcetH-Acet:H_2O**, with a molecular mass of 356.806 g mol^{-1} and anticipated mass reductions of 15.3% and 19.3% for

View Article Online
DOI: 10.1039/D5MR00156K

mono- and di-hydrate forms, respectively, has an experimental reduction of *ca*. 17% over a temperature range from 65 °C to 175 °C, before decomposing at *ca*. 210 °C (**Fig. S25**). As such, **AcetH-Acet:H_2O** is likely a monohydrate and the remainder of the mass loss (~2.7%) is due to the volatilization of surface water molecules. It is also possible that **AcetH-Acet:H_2O** contains a non-stoichiometric amount of water, such as 1.5 water molecules per asymmetric unit, which would result in a 17.4% mass loss.[53]

3.6.3 $^{35/37}$Cl SSNMR. ^{35}Cl SSNMR spectra were acquired for all HCl salts under static conditions at 18.8 T, as well as under MAS conditions at 18.8 T for most samples. In order to accurately determine the EFG and CS tensor parameters, ^{35}Cl SSNMR spectra are usually acquired at two different fields. However, since chlorine has a second NMR-active isotope, ^{37}Cl (I = 3/2), ^{37}Cl SSNMR spectra were acquired for most HCl salts under static conditions at 18.8 T to enable a similar analysis.[48,49,65] MAS experiments, which can average the contributions from CSA, but only partially average those from the SOQI, enable the acquisition of spectra that allow for the facile determination of C_Q, η_Q, and δ_{iso}. In turn, this facilitates simulations of corresponding static NMR spectra (the latter require eight parameters to fit, including the CS tensors and Euler angles that describe the relative orientation of the EFG and CS tensors;[137] see **Table 4** for definitions).

$^{35/37}$Cl SSNMR spectra for each form feature CT patterns that are different from one another, demonstrating the utility of $^{35/37}$Cl SSNMR (*cf.* **Figs. 3 – 5**) for spectral fingerprinting. The magnitudes of C_Q reflect the degree of spherical symmetry of the ground state electron density about the Cl^- ion (increased magnitudes indicate less spherical symmetry), while the η_Q values describe the axial asymmetry of the EFG tensor ($0 \leq \eta_Q \leq 1$, where $\eta_Q = 0$ is axial). All of this, combined with the relatively short acquisition times for these spectra, makes $^{35/37}$Cl SSNMR

View Article Online
DOI: 10.1039/D5MR00156K

an ideal technique for not only obtaining spectral fingerprints, but also for studying the relationships between the $^{35/37}$Cl EFG tensors and hydrogen bonding environments of the chloride ions (**§3.7**).

Select sets of $^{35/37}$Cl SSNMR spectra acquired at 18.8 T are shown in **Fig. 3**. The appearances of the CT patterns are dominated by the SOQI, having breadths ranging from 10 to 150 kHz. All spectra of the known HCl salts feature a single CT pattern corresponding to single distinct chloride site, with the exception of those of **IsoAH** (**Fig. 4),** which feature two overlapping powder patterns, in agreement with its crystal structure.[138] The spectra show no evidence of unwanted side products (*i.e.*, other organic HCl salts or sharp peaks indicating hydrated chloride ions), indicating that the reaction conditions for salt formation are selective for specific products.

We now consider the ^{35}Cl SSNMR spectra from the perspectives of phase identification and structural interpretation, first discussing the HCl salts of **Nic**, **Iso**, **NicA**, and **IsoA** (**Fig. 5A**). **NicH** and **NicH-Nic:H$_2$O** have distinct ^{35}Cl CT powder patterns, with the former arising from a moderate C_Q and low η_Q, and the latter from a small C_Q and high η_Q. **IsoH** and **IsoH-Iso:H$_2$O** are also readily differentiable, as the C_Q for **IsoH** is much smaller, and both EFG tensors are non-axially symmetric. The ^{35}Cl CT patterns of **NicAH** and **IsoAH** are different from those of **NicH** and **IsoH**, with a large C_Q and non-axial η_Q for **NicAH**, and two individual patterns of with moderate C_Q's and variable η_Q's for **IsoAH** (*vide supra*). Second, the HCl salts of **Pic** and **PicA** have very different ^{35}Cl CT patterns from simple salts, hydrates, and hemichlorides (**Fig. 5B**), with the exception of those of **PicAH-PicA** and **PicAH:H$_2$O**, which have powder patterns yielding similar quadrupolar parameters but different values of δ_{iso}. Finally, ^{35}Cl CT patterns for **CaffH** and **CaffH:H$_2$O**, as well as **AcetH:H$_2$O**, **AcetH-Acet**, and **AcetH-Acet:H$_2$O**, all have

View Article Online
DOI: 10.1039/D5MR00156K

unique shapes and distinct sets of quadrupolar and chemical shift parameters (**Fig. 5C**). From this dataset, and a broader review of the data that follows, there are no clear trends in C_Q and η_Q that can be directly related to the general form of the solid (*e.g.*, simple salts do not necessarily have chloride ions with smaller C_Q values or low η_Q values in comparison to their corresponding hydrated forms); rather, differences arise due to the nature of the local Cl^- hydrogen bonding environments (*vide infra*).

3.7 ^{35}Cl EFG tensors and Molecular-Level Structure

Here, we compare the ^{35}Cl EFG tensors derived from quantum chemical computations with those obtained experimentally and consider their relationships with the local structural environment of the chloride ions. Dispersion-corrected plane-wave DFT geometry optimizations [101,102,139] were conducted on structural models based on their respective crystal structures; subsequently, ^{35}Cl EFG tensors were calculated (**Table 4**). A comparison of experimental and computed EFG tensors (**Fig. S26**) shows a reasonable correlation, with an RMS EFG distance (Γ_{EFG}) of 0.66 MHz (see **Supplement S1** for discussion of Γ_{EFG}).[62,102] However, significant outliers are observed for **AcetH-Acet**, **CaffH**, and **CaffH:H_2O**, possibly due to dynamics that partially average their quadrupolar interactions that are not reflected in the DFT calculations, which are conducted on static structural models. To further investigate this, ^{35}Cl spectra of **CaffH:H_2O** and **AcetH-Acet** were acquired at 245 K (**Fig. S27**). In both cases, there is an increase in the magnitudes of both C_Q and η_Q at the lower temperature, bringing experimental and calculated values into better agreement. Removing these outliers from the original correlation plot results in better agreement, with a Γ_{EFG} = 0.51 MHz (**Fig. 6**).

View Article Online
DOI: 10.1039/D5MR00156K

The ^{35}Cl EFG tensors of chloride ions depend on the surrounding H···Cl$^-$ bonds, including their number, their lengths [r(H···Cl$^-$)], the types of moieties involved in bonding, and their spatial arrangement. Some information on H···Cl$^-$ bonds can be garnered directly from the quadrupolar parameters; however, DFT calculations are useful for closely examining these relationships. We note that typical H···Cl$^-$ bonds are classified as having r(H···Cl$^-$) ≤ 2.6 Å;[140] however, it is the short H···Cl$^-$ contacts, *i.e.*, r(H···Cl$^-$) ≲ 2.2 Å, which largely dictate the properties of the ^{35}Cl EFG tensors.[58,61]

Summarizing, the ^{35}Cl EFG tensor orientations, magnitudes and signs of C_Q, and structural relationships are consistent with those from previous reports on a wide range of organic HCl salts (**Table 5**). For systems with one short H···Cl$^-$ or two short H···Cl$^-$ contacts with ∠(H···Cl···H) ≥ 140°, the magnitudes of C_Q are moderate to large, their signs are negative (*i.e.*, positive V_{33} components), and V_{33} is oriented along or near the direction of the shortest contact. In cases with two short contacts, small to moderate magnitudes of C_Q are observed, their signs are positive, with V_{33} oriented approximately perpendicular to the H···Cl$^-$···H planes. Values of r(H···Cl$^-$) are generally found to be shorter for short contacts involving RCOOH moieties than those associated with 1° and 2° amides. The situation becomes more complex for two or three short contacts and additional hydrogen bonds – this is where DFT calculations have great value. Below, we discuss the ^{35}Cl EFG tensors and their orientation (**Figs. 7** and **8**) and the impact of different H···Cl$^-$ contacts, including r(H···Cl$^-$) and the identities of the hydrogen-bonding moieties (**Table 5**).

We begin by comparing **NicAH**, **NicH**, and **NicH-Nic:H$_2$O** (**Fig. 7A**). **NicAH** and **NicH** each have a single short contact, which results in moderate values of C_Q (–6.21 MHz and –4.72 MHz, respectively), with V_{33}, aligning near the axis of the short contact. The magnitude of C_Q is

View Article Online
DOI: 10.1039/D5MR00156K

larger for **NicAH** due to the RCOOH moiety, which generally has shorter r(H···Cl$^-$) values than amide groups, and hence, larger magnitudes of C_Q. **NicH-Nic:H$_2$O** is distinct, with three H···Cl$^-$ bonds in a pyramidal arrangement, leading to a C_Q with a relatively small magnitude (3.52 MHz) and sign opposite to those above, with V_{33} oriented roughly perpendicular to a plane formed by the three hydrogen bonds.

IsoH and **IsoAH** (**Fig. 7B**) have one and two chloride ion sites, respectively. The chloride ion environments all feature two short contacts arranged in "V" formations. The C_Q values are all positive, with larger magnitudes in **IsoAH** because of the RCOOH moieties, which result in shorter values of r(H···Cl$^-$). In all cases, V_{33} is oriented approximately perpendicular to the H···Cl$^-$···H plane.

We next compare **PicH:H$_2$O**, **PicAH:H$_2$O**, **PicAH**, and **PicH**. For the hydrates **PicH:H$_2$O** and **PicAH:H$_2$O**, the C_Q values are positive, with V_{33} oriented perpendicular to the H···Cl$^-$···H planes featuring an RR′NH moiety and H$_2$O molecule (**Fig. 7C**). **PicAH** has a large C_Q = –8.66 MHz and η_Q = 0.0, which results from two short H···Cl$^-$ contacts with hydrogen atoms positioned on opposite sides of the chloride ion,[58,122] and V_{33} aligned closely to the shorter H···Cl$^-$ contact. This stands in contrast with **PicH** (for which the crystal structure is unknown), which has a small experimentally-determined C_Q = 2.25 MHz, suggesting the presence of longer hydrogen bonds with surrounding 1° and 2° amides).

AcetH:H$_2$O and **AcetH-Acet** both have low-to-moderate C_Q values. **AcetH-Acet** has three short H···Cl$^-$ contacts and a low η_Q value (**Fig. 8A**). The C_Q magnitude is due to the comparatively larger number of contacts, whereas the latter results from the pyramidal arrangement of hydrogen bonds that approaches C_3 symmetry. **AcetH:H$_2$O** has two short

View Article Online
DOI: 10.1039/D5MR00156K

contacts and two additional hydrogen bonds with H_2O molecules. In both cases, C_Q is positive and the alignment of V_{33} is roughly perpendicular to the short contacts.

Finally, **CaffH** and **CaffH:H_2O** have distinct chloride ion environments (**Fig. 8B**). **CaffH** has a single short contact (RR′NH), and as expected, a negative, moderate C_Q. However, V_{33} is oriented perpendicular to this bond rather than along it, which is unusual. **CaffH:H_2O** has four hydrogen bonds, two of which are short contacts, all arising from water molecules, which is a coordination motif rarely observed in organic HCl salts. V_{33} is oriented near the shortest hydrogen bond. The uncommon hydrogen bonding networks in **CaffH** and **CaffH:H_2O** may account for the anomalous ^{35}Cl EFG tensor orientations and contribute to the discrepancies between calculated and experimental NMR parameters; for **CaffH:H_2O**, this may also be the result of dynamical motions of the water molecules that influence the experimentally measured ^{35}Cl EFGs.

View Article Online
DOI: 10.1039/D5MR00156K

4. Conclusions

This study demonstrated the (i) rapid and quantitative mechanochemical syntheses of sixteen HCl salts, including anhydrous forms, hydrates, and hemihydrochlorides (five of which are novel), as well as the formation of **PicH:H_2O** via slow evaporation; (ii) advantages of mechanochemical salification, including negligible waste, minimal solvent use, quantitative yields, accelerated discovery of solid forms, and scalability; (iii) complexities inherent to solid-state chemistry, where common assumptions and behaviors derived from solution chemistry do not apply (*e.g.*, a myriad of factors can influence kinetic *vs*. thermodynamic products and the limitations of using pK_a's to make predictions regarding protonation of pyridyl nitrogens; (iv) value of $^{35/37}$Cl SSNMR spectroscopy for fingerprinting of chloride salts, impurity detection, and structural elucidation; and (v) the application of plane-wave DFT calculations of ^{35}Cl EFG tensors to investigate their relationships to the hydrogen bonding environments of chloride ions.

The combination of mechanochemical salification and characterization via $^{35/37}$Cl SSNMR offers substantial benefits at both laboratory and industrial scales. On the laboratory side of things, screening for solid forms is significantly accelerated, making the discovery and identification of rare solid forms, such as hemihydrochlorides, more straightforward. At an industrial scale, mechanochemistry has great potential for increased efficiency and reduced costs, which benefits the manufacturer and consumer, due to reduction in solvent, energy use, safety hazards, waste disposal, and unwanted by-products. The usefulness of $^{35/37}$Cl SSNMR in laboratory settings is clear from this work and many preceding accounts; however, it could play an important role in industrial settings for spectral fingerprinting and impurity detection, especially since MAS experiments are not absolutely required (this eliminates the costs of rotors, tedious sample packing, and opens the possibility of looking at complex dosage formulations like

View Article Online
DOI: 10.1039/D5MR00156K

pills and capsules directly) – and, only a single magnetic field is necessary.[57,141] Furthermore, it could aid in the quantification of HCl salts, examination of disproportion,[142] and streamlining of early-stage screening and selection, all of which are essential for time-sensitive discovery and in formulation pipelines, where rapid decisions on salt forms are needed prior to scaling up or advancing through regulatory pathways.

While the current work focuses specifically on organic HCl salts, this mechanochemical salification method is broadly applicable to a wider range of APIs. The same principles could be extended to form salts with polyprotic acids (*e.g.*, H_2SO_4, H_3PO_4, *etc*.) or other pharmaceutically relevant counterions (*e.g.*, HBr, HNO_3, methanesulfonic acid, *etc*.), potentially enabling the rapid generation of diverse salt forms beyond those traditionally accessed via solution-based methods. This versatility highlights the utility of mechanochemistry for the development of many new solid forms across a vast landscape of APIs.

View Article Online
DOI: 10.1039/D5MR00156K

Conflict of Interest

The authors have no conflict of interest to declare.

Acknowledgements

The authors thank the Florida State University and the National High Magnetic Field Laboratory for funding this research. The National High Magnetic Field Laboratory is supported by the National Science Foundation through NSF/DMR-2128556, NSF/DMR-1644779, and the State of Florida. The authors thank Jason Kitchen and Peter Gor'kov for configuring probes for ^{37}Cl NMR experimentation, and the staff at the National High Magnetic Field Laboratory for their continued support. A portion of this research used resources provided by the X-ray Crystallography Center and the Materials Characterization Laboratory at the FSU Department of Chemistry and Biochemistry. V.K.R. is grateful to the NSF Research Experiences for Undergraduates (REU) program for supporting a term of summer research at the FSU and the NHMFL.

View Article Online
DOI: 10.1039/D5MR00156K

References

(1) Hamaed, H.; Pawlowski, J. M.; Cooper, B. F. T. T.; Fu, R.; Eichhorn, S. H.; Schurko, R. W. Application of Solid-State 35Cl NMR to the Structural Characterization of Hydrochloride Pharmaceuticals and Their Polymorphs. *J Am Chem Soc* **2008**, *130*, 11056–11065. https://doi.org/10.1021/ja802486q.

(2) Paulekuhn, G. S.; Dressman, J. B.; Saal, C. Trends in Active Pharmaceutical Ingredient Salt Selection Based on Analysis of the Orange Book Database. *J Med Chem* **2007**, *50*, 6665–6672. https://doi.org/10.1021/JM701032Y.

(3) Muleva, C. T.; Bharate, S. S. Halide Counterions in FDA-Approved Pharmaceutical Salts. *J Drug Deliv Sci Technol* **2023**, *89*, 104999. https://doi.org/10.1016/J.JDDST.2023.104999.

(4) Bharate, S. S. Recent Developments in Pharmaceutical Salts: FDA Approvals from 2015 to 2019. *Drug Discov Today* **2021**, *26*, 384–398. https://doi.org/10.1016/J.DRUDIS.2020.11.016.

(5) Hossain Mithu, M. S.; Economidou, S.; Trivedi, V.; Bhatt, S.; Douroumis, D. Advanced Methodologies for Pharmaceutical Salt Synthesis. *Cryst Growth Des* **2021**, *21*, 1358–1374. https://doi.org/https://doi.org/10.1021/acs.cgd.0c01427.

(6) Noble, E. G.; Shanks, D. E. Hydrogen Chloride and Hydrogen Bromide Sparging Crystallization of Chloride and Bromide Metal Salts. *Crystallization and Precipitation* **1987**, 89–98. https://doi.org/10.1016/B978-0-08-035751-5.50019-2.

(7) Perumalla, S. R.; Sun, C. C. Confused HCl: Hydrogen Chloride or Hydrochloric Acid? *Chemistry – A European Journal* **2012**, *18*, 6462–6464. https://doi.org/10.1002/CHEM.201103669.

(8) Perumalla, S. R.; Shi, L.; Sun, C. C. Ionized Form of Acetaminophen with Improved Compaction Properties. *CrystEngComm* **2012**, *14*, 2389–2390. https://doi.org/10.1039/C1CE06278F.

(9) Slouf, M. 3-Carboxypyridinium Chloride. *Acta Crystallogr Sect E Struct Rep Online* **2001**, *57*, o61–o62. https://doi.org/10.1107/S1600536800019632.

(10) Fellows, S. M.; Prior, T. J. Crystal Structure of 4-Carbamoylpyridinium Chloride. *Acta Crystallogr E Crystallogr Commun* **2016**, *72*, 436–439. https://doi.org/10.1107/S2056989016003340.

(11) Laurent, A.; IUCr. Structure Cristalline Du Chlorhydrate de l'acide Picolique. *Acta Cryst.* **1965**, *18*, 799–806. https://doi.org/10.1107/S0365110X65001809.

(12) Gubin, A.; Nurakhmetov, N.; Buranbaev, M.; Mulkina, R.; Erkasov, R. Crystal and Molecular-Structure of Nicotinamide Hydrochloride - Donor-Acceptor Properties of Protonated Nicotinamide. *Kristallografiya* **1989**, 238–239.

(13) Mercer, A.; Trotter, J.; IUCr. Crystal and Molecular Structure of 1,3,7-Trimethyl-2,6-Purinedione Hydrochloride Dihydrate (Caffeine Hydrochloride Dihydrate). *Acta Cryst.* **1978**, *34*, 450–453. https://doi.org/10.1107/S0567740878003337.

(14) Adams, C. J.; Angeloni, A.; Orpen, A. G.; Podesta, T. J.; Shore, B. Crystal Synthesis of Organic-Inorganic Hybrid Salts Based on Tetrachloroplatinate and -Palladate Salts of Organic Cations:

View Article Online
DOI: 10.1039/D5MR00156K

Formation of Linear, Two-, and Three-Dimensional NH···Cl Hydrogen Bond Networks. *Cryst Growth Des* **2006**, *6*, 411–422. https://doi.org/https://doi.org/10.1021/cg050362o.

(15) Smith, G.; Byriel, K. A.; Kennard, C. H. L.; IUCr. 2-Carboxypyridinium Chloride Monohydrate. *Acta Cryst.* **1995**, *C51*, 1425–1427. https://doi.org/10.1107/S0108270195000175.

(16) Nakagawa, K.; Murakami, W.; Andrieu, J.; Vessot, S. Freezing Step Controls the Mannitol Phase Composition Heterogeneity. *Chemical Engineering Research and Design* **2009**, *87*, 1017–1027. https://doi.org/10.1016/J.CHERD.2009.01.008.

(17) Lee, S.; Wi, H. S.; Jo, W.; Cho, Y. C.; Lee, H. H.; Jeong, S. Y.; Kim, Y. Il; Lee, G. W. Multiple Pathways of Crystal Nucleation in an Extremely Supersaturated Aqueous Potassium Dihydrogen Phosphate (KDP) Solution Droplet. *Proc Natl Acad Sci U S A* **2016**, *113*, 13618–13623. https://doi.org/doi.org/10.1073/pnas.1604938113.

(18) Mejri, E.; Bouhlila, R.; Helmig, R. Heterogeneity Effects on Evaporation-Induced Halite and Gypsum Co-Precipitation in Porous Media. *Transp Porous Media* **2017**, *118*, 39–64. https://doi.org/doi.org/10.1007/s11242-017-0846-8.

(19) Pagola, S. Outstanding Advantages, Current Drawbacks, and Significant Recent Developments in Mechanochemistry: A Perspective View. *Crystals (Basel)* **2023**, *13*, 124. https://doi.org/10.3390/CRYST13010124.

(20) Friščić, T.; Mottillo, C.; Titi, H. M. Mechanochemistry for Synthesis. *Angewandte Chemie - International Edition* **2019**, 1018–1029. https://doi.org/10.1002/anie.201906755.

(21) Do, J.-L.; Friščić, T. Mechanochemistry: A Force of Synthesis. *ACS Cent Sci* **2017**, *3*, 13–19. https://doi.org/10.1021/acscentsci.6b00277.

(22) Crawford, D. E.; Miskimmin, C. K. G.; Albadarin, A. B.; Walker, G.; James, S. L. Organic Synthesis by Twin Screw Extrusion (TSE): Continuous, Scalable and Solvent-Free. *Green Chemistry* **2017**, *19*, 1507–1518. https://doi.org/10.1039/C6GC03413F.

(23) Rensch, T.; Chantrain, V.; Sander, M.; Grätz, S.; Borchardt, L. Scale-Up of Solvent-Free, Mechanochemical Precursor Synthesis for Nanoporous Carbon Materials via Extrusion. *ChemSusChem* **2022**, *15*, e202200651. https://doi.org/10.1002/CSSC.202200651.

(24) Stolar, T.; Lukin, S.; Tireli, M.; Sović, I.; Karadeniz, B.; Kereković, I.; Matijašić, G.; Gretić, M.; Katančić, Z.; Dejanović, I.; Michiel, M. Di; Halasz, I.; Užarević, K. Control of Pharmaceutical Cocrystal Polymorphism on Various Scales by Mechanochemistry: Transfer from the Laboratory Batch to the Large-Scale Extrusion Processing. *ACS Sustain Chem Eng* **2019**, *7*, 7102–7110. https://doi.org/10.1021/acssuschemeng.9b00043.

(25) Stolle, A.; Schmidt, R.; Jacob, K. Scale-up of Organic Reactions in Ball Mills: Process Intensification with Regard to Energy Efficiency and Economy of Scale. *Faraday Discuss* **2014**, *170*, 267–286. https://doi.org/10.1039/C3FD00144J.

(26) Madanayake, S. N.; Manipura, A.; Thakuria, R.; Adassooriya, N. M. Opportunities and Challenges in Mechanochemical Cocrystallization toward Scaled-Up Pharmaceutical Manufacturing. *Org Process Res Dev* **2023**, *27*, 409–422. https://doi.org/https://doi.org/10.1021/acs.oprd.2c00314.

View Article Online
DOI: 10.1039/D5MR00156K

(27) Jan-Hendrik Schöbel; Frederik Winkelmann; Joel Bicker; Michael Felderhoff. Mechanochemical Kilogram-Scale Synthesis of Rac -Ibuprofen:Nicotinamide Co-Crystals Using a Drum Mill. *RSC Mechanochemistry* **2025**, *2*, 224–229. https://doi.org/10.1039/D4MR00096J.

(28) Germann, L. S.; Arhangelskis, M.; Etter, M.; Dinnebier, R. E.; Friščić, T. Challenging the Ostwald Rule of Stages in Mechanochemical Cocrystallisation. *Chem Sci* **2020**, *11*, 10092–10100. https://doi.org/10.1039/d0sc03629c.

(29) Braga, D.; Giaffreda, S. L.; Grepioni, F.; Pettersen, A.; Maini, L.; Curzi, M.; Polito, M. Mechanochemical Preparation of Molecular and Supramolecular Organometallic Materials and Coordination Networks. *Dalton Transactions* **2006**, *6*, 1249–1263. https://doi.org/10.1039/B516165G.

(30) Frisić, T.; Childs, S. L.; Rizvi, S. A. A.; Jones, W. The Role of Solvent in Mechanochemical and Sonochemical Cocrystal Formation: A Solubility-Based Approach for Predicting Cocrystallisation Outcome. *CrystEngComm* **2009**, *11*, 418–426. https://doi.org/10.1039/B815174A.

(31) Crawford, D. E.; Casaban, J.; Crawford, D. E.; Casaban, J. Recent Developments in Mechanochemical Materials Synthesis by Extrusion. *Advanced Materials* **2016**, *28*, 5747–5754. https://doi.org/10.1002/ADMA.201505352.

(32) Lennox, C. B.; Borchers, T. H.; Gonnet, L.; Barrett, C. J.; Koenig, S. G.; Nagapudi, K.; Friščić, T. Direct Mechanocatalysis by Resonant Acoustic Mixing (RAM). *Chem Sci* **2023**, *14*, 7475–7481. https://doi.org/10.1039/D3SC01591B.

(33) Michalchuk, A. A. L.; Hope, K. S.; Kennedy, S. R.; Blanco, M. V.; Boldyreva, E. V.; Pulham, C. R. Ball-Free Mechanochemistry: In Situ Real-Time Monitoring of Pharmaceutical Co-Crystal Formation by Resonant Acoustic Mixing. *Chemical Communications* **2018**, *54*, 4033–4036. https://doi.org/10.1039/C8CC02187B.

(34) Teoh, Y.; Ayoub, G.; Huskić, I.; Titi, H. M.; Nickels, C. W.; Herrmann, B.; Friščić, T. SpeedMixing: Rapid Tribochemical Synthesis and Discovery of Pharmaceutical Cocrystals without Milling or Grinding Media**. *Angewandte Chemie International Edition* **2022**, *61*. https://doi.org/10.1002/anie.202206293.

(35) Anastas, P.; Eghbali, N. Green Chemistry: Principles and Practice. *Chem. Soc. Rev.* **2010**, *39*, 301–312. https://doi.org/10.1039/B918763B.

(36) Ardila-Fierro, K. J.; Hernández, J. G. Sustainability Assessment of Mechanochemistry by Using the Twelve Principles of Green Chemistry. *ChemSusChem* **2021**, *14*, 2145–2162. https://doi.org/10.1002/CSSC.202100478.

(37) Geppi, M.; Mollica, G.; Borsacchi, S.; Veracini, C. A. Solid-State NMR Studies of Pharmaceutical Systems. *Appl Spectrosc Rev* **2008**, *43*, 202–302. https://doi.org/10.1080/05704920801944338.

(38) Harris, R. K. NMR Studies of Organic Polymorphs & Solvates. *Analyst* **2006**, *131*, 351–373. https://doi.org/10.1039/B516057J.

(39) Pindelska, E.; Sokal, A.; Kolodziejski, W. Pharmaceutical Cocrystals, Salts and Polymorphs: Advanced Characterization Techniques. *Adv Drug Deliv Rev* **2017**, *117*, 111–146. https://doi.org/10.1016/J.ADDR.2017.09.014.

View Article Online
DOI: 10.1039/D5MR00156K

(40) Stephenson, G. A.; Forbes, R. A.; Reutzel-Edens, S. M. Characterization of the Solid State: Quantitative Issues. *Adv Drug Deliv Rev* **2001**, *48*, 67–90. https://doi.org/10.1016/S0169-409X(01)00099-0.

(41) Vogt, F. G. Solid-State NMR in Drug Discovery and Development. In *New Applications of NMR in Drug Discovery and Development*; 2013; pp 43–100. https://doi.org/10.1039/9781849737661-00043.

(42) Brittain, H. G. *Spectroscopy of Pharmaceutical Solids*; CRC Press, 2006. https://doi.org/10.1201/9780849361333.

(43) Shankland, K. An Overview of Powder X-Ray Diffraction and Its Relevance to Pharmaceutical Crystal Structures. **2016**, 293–314. https://doi.org/10.1007/978-1-4939-4029-5_8.

(44) Brittain, H. G.; Bogdanowich, S. J.; Bugay, D. E.; DeVincentis, J.; Lewen, G.; Newman, A. W. Physical Characterization of Pharmaceutical Solids. *Pharm Res* **1991**, *8*, 963–973. https://doi.org/10.1023/A:1015888520352/.

(45) Bugay, D. E. Characterization of the Solid-State: Spectroscopic Techniques. *Adv Drug Deliv Rev* **2001**, *48*, 43–65. https://doi.org/10.1016/S0169-409X(01)00101-6.

(46) Namespetra, A. M.; Hirsh, D. A.; Hildebrand, M. P.; Sandre, A. R.; Hamaed, H.; Rawson, J. M.; Schurko, R. W. 35Cl Solid-State NMR Spectroscopy of HCl Pharmaceuticals and Their Polymorphs in Bulk and Dosage Forms. *CrystEngComm* **2016**, *18*, 6213–6232. https://doi.org/10.1039/c6ce01069e.

(47) Bryce, D. L.; Sward, G. D. Chlorine-35/37 NMR Spectroscopy of Solid Amino Acid Hydrochlorides: Refinement of Hydrogen-Bonded Proton Positions Using Experiment and Theory. *J Phys Chem B* **2006**, *110*, 26461–26470. https://doi.org/10.1021/jp065878c.

(48) Szell, P. M. J.; Bryce, D. L. 35Cl Solid-State NMR and Computational Study of Chlorine Halogen Bond Donors in Single-Component Crystalline Chloronitriles. *J. Phys. Chem. C* **2016**, *120*, 11121–11130. https://doi.org/10.1021/acs.jpcc.6b02806.

(49) Struppe, J.; Quinn, C. M.; Sarkar, S.; Gronenborn, A. M.; Polenova, T. Ultrafast 1 H MAS NMR Crystallography for Natural Abundance Pharmaceutical Compounds. *Mol Pharm* **2020**, *17*, 674–682. https://doi.org/10.1021/acs.molpharmaceut.9b01157.

(50) Vogt, F. G.; Williams, G. R.; Strohmeier, M.; Johnson, M. N.; Copley, R. C. B. Solid-State NMR Analysis of a Complex Crystalline Phase of Ronacaleret Hydrochloride. *Journal of Physical Chemistry B* **2014**, *118*, 10266–10284. https://doi.org/https://doi.org/10.1021/jp505061j.

(51) Pandey, M. K.; Kato, H.; Ishii, Y.; Nishiyama, Y. Two-Dimensional Proton-Detected 35Cl/1H Correlation Solid-State NMR Experiment under Fast Magic Angle Sample Spinning: Application to Pharmaceutical Compounds. *Physical Chemistry Chemical Physics* **2016**, *18*, 6209–6216. https://doi.org/10.1039/C5CP06042G.

(52) Stirk, A. J.; Holmes, S. T.; Souza, F. E. S.; Hung, I.; Gan, Z.; Britten, J. F.; Rey, A. W.; Schurko, R. W. An Unusual Ionic Cocrystal of Ponatinib Hydrochloride: Characterization by Single-Crystal X-Ray Diffraction and Ultra-High Field NMR Spectroscopy. *CrystEngComm* **2024**, *26*, 1219–1233. https://doi.org/10.1039/D3CE01062G.

View Article Online
DOI: 10.1039/D5MR00156K

(53) Hildebrand, M.; Hamaed, H.; Namespetra, A. M.; Donohue, J. M.; Fu, R.; Hung, I.; Gan, Z.; Schurko, R. W. 35 Cl Solid-State NMR of HCl Salts of Active Pharmaceutical Ingredients: Structural Prediction, Spectral Fingerprinting and Polymorph Recognition. *CrystEngComm* **2014**, *16*, 7334–7356. https://doi.org/10.1039/C4CE00544A.

(54) Abdulla, L. M.; Peach, A. A.; Holmes, S. T.; Dowdell, Z. T.; Watanabe, L. K.; Iacobelli, E. M.; Hirsh, D. A.; Rawson, J. M.; Schurko, R. W. Synthesis and Characterization of Xylazine Hydrochloride Polymorphs, Hydrates, and Cocrystals: A 35Cl Solid-State NMR and DFT Study. *Cryst Growth Des* **2023**, *23*, 3412–3426. https://doi.org/10.1021/acs.cgd.2c01539.

(55) Hirsh, D. A.; Holmes, S. T.; Chakravarty, P.; Peach, A. A.; Dipasquale, A. G.; Nagapudi, K.; Schurko, R. W. In Situ Characterization of Waters of Hydration in a Variable-Hydrate Active Pharmaceutical Ingredient Using 35Cl Solid-State NMR and X-Ray Diffraction. *Cryst Growth Des* **2019**, *19*, 7349–7362. https://doi.org/10.1021/acs.cgd.9b01218.

(56) Holmes, S. T.; Hook, J. M.; Schurko, R. W. Nutraceuticals in Bulk and Dosage Forms: Analysis by 35Cl and 14N Solid-State NMR and DFT Calculations. *Mol Pharm* **2022**, *19*, 440–455. https://doi.org/10.1021/ACS.MOLPHARMACEUT.1C00708.

(57) Peach, A. A.; Hirsh, D. A.; Holmes, S. T.; Schurko, R. W. Mechanochemical Syntheses and 35 Cl Solid-State NMR Characterization of Fluoxetine HCl Cocrystals. *CrystEngComm* **2018**, *20*, 2780–2792. https://doi.org/10.1039/C8CE00378E.

(58) Dowdell, Z. T.; Peach, A. A.; Purdie, J. P.; Holmes, S. T.; Watanabe, L. K.; Rawson, J. M.; Schurko, R. W. Mechanochemical Synthesis and 35 Cl NMR Crystallography of Ionic Cocrystals of Phenothiazine Drugs. *CrystEngComm* **2025**, *27*, 3752–3768. https://doi.org/10.1039/D5CE00426H.

(59) Vojvodin, C. S.; Sanchez, J. E.; Holmes, S. T.; Lin, X.; Schurko, R. W. Mechanochemical Synthesis and NMR Crystallography of Multicomponent Crystals: New Perspectives from Chlorine and Alkali Metal Solid-State NMR Spectroscopy. *Cryst Growth Des* **2025**, *25*, 9591–9609. https://doi.org/10.1021/ACS.CGD.5C00540.

(60) Vojvodin, C. S.; Holmes, S. T.; Watanabe, L. K.; Rawson, J. M.; Schurko, R. W. Multi-Component Crystals Containing Urea: Mechanochemical Synthesis and Characterization by 35 Cl Solid-State NMR Spectroscopy and DFT Calculations. *CrystEngComm* **2022**, *24*, 2626–2641. https://doi.org/10.1039/D1CE01610E.

(61) A. Peach, A.; H. Fleischer, C.; Kirill Levin; T. Holmes, S.; E. Sanchez, J.; W. Schurko, R. Quadrupolar NMR Crystallography Guided Crystal Structure Prediction (QNMRX-CSP). *CrystEngComm* **2024**, *26*, 4782–4803. https://doi.org/10.1039/D3CE01306E.

(62) H. Fleischer, C.; T. Holmes, S.; Kirill Levin; L. Veinberg, S.; W. Schurko, R. Characterization of Ephedrine HCl and Pseudoephedrine HCl Using Quadrupolar NMR Crystallography Guided Crystal Structure Prediction. *Faraday Discuss* **2025**, *255*, 88–118. https://doi.org/10.1039/D4FD00089G.

(63) Bryce, D. L.; Sward, G. D. Solid-State NMR Spectroscopy of the Quadrupolar Halogens: Chlorine-35/37, Bromine-79/81, and Iodine-127. *Magnetic Resonance in Chemistry* **2006**, *44*, 409–450. https://doi.org/10.1002/MRC.1741.

View Article Online
DOI: 10.1039/D5MR00156K

(64) Perras, F. A.; Bryce, D. L.; Perras, F. A.; Bryce, D. L. Direct Investigation of Covalently Bound Chlorine in Organic Compounds by Solid-State 35Cl NMR Spectroscopy and Exact Spectral Line-Shape Simulations. *Angewandte Chemie International Edition* **2012**, *51*, 4227–4230. https://doi.org/10.1002/ANIE.201200728.

(65) Bryce, D. L.; Sward, G. D. Chlorine-35/37 NMR Spectroscopy of Solid Amino Acid Hydrochlorides: Refinement of Hydrogen-Bonded Proton Positions Using Experiment and Theory. *J Phys Chem B* **2006**, *110*, 26461–26470. https://doi.org/10.1021/jp065878c.

(66) Bryce, D. L.; Gee, M.; Wasylishen, R. E. High-Field Chlorine NMR Spectroscopy of Solid Organic Hydrochloride Salts: A Sensitive Probe of Hydrogen Bonding Environment. *J Phys Chem A* **2001**, *105*, 10413–10421. https://doi.org/10.1021/jp011962a.

(67) Chapman, R. P.; Widdifield, C. M.; Bryce, D. L. Solid-State NMR of Quadrupolar Halogen Nuclei. *Prog Nucl Magn Reson Spectrosc* **2009**, *55*, 215–237. https://doi.org/10.1016/J.PNMRS.2009.05.001.

(68) Chapman, R. P.; Hiscock, J. R.; Gale, P. A.; Bryce, D. L. A Solid-State 35/37Cl NMR Study of a Chloride Ion Receptor and a GIPAW-DFT Study of Chlorine NMR Interaction Tensors in Organic Hydrochlorides. *Can J Chem* **2011**, *89*, 822–834. https://doi.org/doi.org/10.1139/v10-177.

(69) Bryce, D. L.; Sward, G. D.; Adiga, S. Solid-State 35/37Cl NMR Spectroscopy of Hydrochloride Salts of Amino Acids Implicated in Chloride Ion Transport Channel Selectivity: Opportunities at 900 MHz. *J Am Chem Soc* **2006**, *128*, 2121–2134. https://doi.org/doi.org/10.1021/ja057253i.

(70) Perumalla, S. R.; Sun, C. C. Design and Synthesis of Solid State Structures with Conjugate Acid-Base Pair Interactions. *CrystEngComm* **2012**, *14*, 3851–3853. https://doi.org/10.1039/C2CE25193K/.

(71) Takusagawa, F.; Shimada, A. Isonicotinic Acid. *Acta Cryst.* **1976**, *B32*, 1925–1927. https://doi.org/10.1107/S0567740876006754.

(72) Wright, W. B.; King, G. S. D. The Crystal Structure of Nicotinic Acid. *Acta Cryst.* **1953**, *6*, 305–317. https://doi.org/10.1107/S0365110X53000867.

(73) Miwa, Y.; Mizuno, T.; Tsuchida, K.; Taga, T.; Iwata, Y. Experimental Charge Density and Electrostatic Potential in Nicotinamide. *Acta Cryst.* **1999**, *B55*, 78–84. https://doi.org/10.1107/S0108768198007848.

(74) Aakeröy, C. B.; Beatty, A. M.; Helfrich, B. A.; Nieuwenhuyzen, M. Do Polymorphic Compounds Make Good Cocrystallizing Agents? A Structural Case Study That Demonstrates the Importance of Synthon Flexibility. *Cryst Growth Des* **2003**, *3*, 159–165. https://doi.org/doi.org/10.1021/cg025593z.

(75) Tyler, A. R.; Ragbirsingh, R.; McMonagle, C. J.; Waddell, P. G.; Heaps, S. E.; Steed, J. W.; Thaw, P.; Hall, M. J.; Probert, M. R. Encapsulated Nanodroplet Crystallization of Organic-Soluble Small Molecules. *Chem* **2020**, *6*, 1755–1765. https://doi.org/10.1016/J.CHEMPR.2020.04.009.

(76) Anitha, R.; Gunasekaran, M.; Kumar, S. S.; Athimoolam, S.; Sridhar, B. Single Crystal XRD, Vibrational and Quantum Chemical Calculation of Pharmaceutical Drug Paracetamol: A New Synthesis Form. *Spectrochim Acta A Mol Biomol Spectrosc* **2015**, *150*, 488–498. https://doi.org/10.1016/J.SAA.2015.05.091.

View Article Online
DOI: 10.1039/D5MR00156K

(77) Takusagawa, F.; Shimada, A. The Crystal Structure of Picolinic Acid. *Chem Lett* **1973**, *2*, 1089–1090. https://doi.org/10.1246/CL.1973.1089.

(78) Takano, T.; Sasada, Y.; Kakudo, M. The Crystal and Molecular Structure of Picolinamide. *Acta Cryst.* **1966**, *21*, 514–522. https://doi.org/10.1107/S0365110X66003396.

(79) David, W. I. F.; Shankland, K. Routine Determination of Molecular Crystal Structures from Powder Diffraction Data. *Chemical Communications* **1998**, *8*, 931–932. https://doi.org/10.1039/A800855H.

(80) CrystalDiffract Overview http://crystalmaker.com/crystaldiffract/ (accessed 2022 -11 -11).

(81) Sheldrick, G. M.; IUCr. SHELXT – Integrated Space-Group and Crystal-Structure Determination. *Acta Cryst.* **2015**, *71*, 3–8. https://doi.org/10.1107/S2053273314026370.

(82) Sheldrick, G. M. Crystal Structure Refinement with SHELXL. *Acta Cryst* **2015**, *71*, 3–8. https://doi.org/10.1107/S2053229614024218.

(83) Hahn, E. L. Spin Echoes. *Physical Review* **1950**, *80*, 580. https://doi.org/10.1103/PhysRev.80.580.

(84) Larsen, F. H.; Jakobsen, H. J.; Ellis, P. D.; Nielsen, N. C. QCPMG-MAS NMR of Half-Integer Quadrupolar Nuclei. *Journal of Magnetic Resonance* **1998**, *131*, 144–147. https://doi.org/10.1006/JMRE.1997.1341.

(85) Larsen, F. H.; Jakobsen, H. J.; Ellis, P. D.; Nielsen, N. C. Sensitivity-Enhanced Quadrupolar-Echo NMR of Half-Integer Quadrupolar Nuclei. Magnitudes and Relative Orientation of Chemical Shielding and Quadrupolar Coupling Tensors. *Journal of Physical Chemistry A* **1997**, *101*, 8597–8606. https://doi.org/10.1021/jp971547b.

(86) Hung, I.; Gan, Z. On the Practical Aspects of Recording Wideline QCPMG NMR Spectra. *Journal of Magnetic Resonance* **2010**, *204*, 256–265. https://doi.org/10.1016/J.JMR.2010.03.001.

(87) Lipton, A. S.; Sears, J. A.; Ellis, P. D. A General Strategy for the NMR Observation of Half-Integer Quadrupolar Nuclei in Dilute Environments. *Journal of Magnetic Resonance* **2001**, *151*, 48–59. https://doi.org/10.1006/JMRE.2001.2353.

(88) Siegel, R.; Nakashima, T. T.; Wasylishen, R. E. Application of Multiple-Pulse Experiments to Characterize Broad NMR Chemical-Shift Powder Patterns from Spin-1/2 Nuclei in the Solid State. *J. Phys. Chem. B* **2004**, *108*, 2218–2226. https://doi.org/10.1021/jp031048c.

(89) Hung, I.; Rossini, A. J.; Schurko, R. W. Application of the Carr-Purcell Meiboom-Gill Pulse Sequence for the Acquisition of Solid-State NMR Spectra of Spin-1/2 Nuclei. *J. Phys. Chem. A* **2004**, *108*, 7112–7120. https://doi.org/doi.org/10.1021/jp0401123.

(90) O'Dell, L. A. The WURST Kind of Pulses in Solid-State NMR. *Solid State Nucl Magn Reson* **2013**, *55–56*, 28–41. https://doi.org/10.1016/J.SSNMR.2013.10.003.

(91) O'Dell, L. A.; Schurko, R. W. QCPMG Using Adiabatic Pulses for Faster Acquisition of Ultra-Wideline NMR Spectra. *Chem Phys Lett* **2008**, *464*, 97–102. https://doi.org/10.1016/J.CPLETT.2008.08.095.

View Article Online
DOI: 10.1039/D5MR00156K

(92) O'Dell, L. A.; Rossini, A. J.; Schurko, R. W.; O'Dell, L. A.; Rossini, A. J.; Schurko, R. W. Acquisition of Ultra-Wideline NMR Spectra from Quadrupolar Nuclei by Frequency Stepped WURST–QCPMG. *Chem Phys Lett* **2009**, *468*, 330–335.

(93) Larsen, F. H.; Jakobsen, H. J.; Ellis, P. D.; Nielsen, N. C. QCPMG-MAS NMR of Half-Integer Quadrupolar Nuclei. *Journal of Magnetic Resonance* **1998**, *131*, 144–147. https://doi.org/10.1006/JMRE.1997.1341.

(94) Bloch, F. Nuclear Induction. *Physical Review* **1946**, *70*, 460–474. https://doi.org/10.1103/PHYSREV.70.460.

(95) Comellas, G.; Lopez, J. J.; Nieuwkoop, A. J.; Lemkau, L. R.; Rienstra, C. M. Straightforward, Effective Calibration of SPINAL-64 Decoupling Results in the Enhancement of Sensitivity and Resolution of Biomolecular Solid-State NMR. *Journal of Magnetic Resonance* **2011**, *209*, 131–135. https://doi.org/10.1016/J.JMR.2010.12.011.

(96) van Meerten, S. G. J.; Franssen, W. M. J.; Kentgens, A. P. M. SsNake: A Cross-Platform Open-Source NMR Data Processing and Fitting Application. *Journal of Magnetic Resonance* **2019**, *301*, 56–66. https://doi.org/10.1016/J.JMR.2019.02.006.

(97) Eichele, K. WSolids1 ver. 1.21.7 http://anorganik.uni-tuebingen.de/klaus/soft/index.php?p=wsolids1/wsolids1.

(98) Perras, F. A.; Paterson, A. L. Automatic Fitting of Multiple-Field Solid-State NMR Spectra. *Solid State Nucl Magn Reson* **2024**, *131*, 101935. https://doi.org/10.1016/J.SSNMR.2024.101935.

(99) David, W. I. F.; Shankland, K.; Shankland, N. Routine Determination of Molecular Crystal Structures from Powder Diffraction Data. *Chemical Communications* **1998**, No. 8, 931–932. https://doi.org/10.1039/A800855H.

(100) Holmes, S. T.; Schurko, R. W. Refining Crystal Structures with Quadrupolar NMR and Dispersion-Corrected Density Functional Theory. *J. Phys. Chem. C* **2018**, *122*, 1809–1820. https://doi.org/10.1021/acs.jpcc.7b12314.

(101) Holmes, S. T.; Vojvodin, C. S.; Schurko, R. W. Dispersion-Corrected DFT Methods for Applications in Nuclear Magnetic Resonance Crystallography. *J. Phys. Chem. A* **2020**, *124*, 10312–10323. https://doi.org/10.1021/acs.jpca.0c06372.

(102) Payne, M. C.; Teter, M. P.; Allan, D. C.; Arias, T. A.; Joannopoulos, J. D. Iterative Minimization Techniques for *Ab Initio* Total-Energy Calculations: Molecular Dynamics and Conjugate Gradients. *Rev Mod Phys* **1992**, *64*, 1045. https://doi.org/10.1103/RevModPhys.64.1045.

(103) Clark, S. J.; Segall, M. D.; Pickard, C. J.; Hasnip, P. J.; Probert, M. I. J.; Refson, K.; Payne, M. C. First Principles Methods Using CASTEP. *Z Kristallogr Cryst Mater* **2005**, *220*, 567–570. https://doi.org/10.1524/zkri.220.5.567.65075.

(104) Hammer, B.; Hansen, L. B.; Nørskov, J. K. Improved Adsorption Energetics within Density-Functional Theory Using Revised Perdew-Burke-Ernzerhof Functionals. *Phys Rev B* **1999**, *59*, 7413. https://doi.org/10.1103/PhysRevB.59.7413.

View Article Online
DOI: 10.1039/D5MR00156K

(105) Yates, J. R.; Pickard, C. J.; Mauri, F. Calculation of NMR Chemical Shifts for Extended Systems Using Ultrasoft Pseudopotentials. *Phys Rev B* **2007**, *76*, 024401. https://doi.org/10.1103/PhysRevB.76.024401.

(106) Pfrommer, B. G.; Côté, M.; Louie, S. G.; Cohen, M. L. Relaxation of Crystals with the Quasi-Newton Method. *J Comput Phys* **1997**, *131*, 233–240. https://doi.org/10.1006/JCPH.1996.5612.

(107) Grimme, S. Semiempirical GGA-Type Density Functional Constructed with a Long-Range Dispersion Correction. *J Comput Chem* **2006**, *27*, 1787–1799. https://doi.org/10.1002/jcc.20495.

(108) McNellis, E. R.; Meyer, J.; Reuter, K. Azobenzene at Coinage Metal Surfaces: Role of Dispersive van Der Waals Interactions. *Phys Rev B Condens Matter Mater Phys* **2009**, *80*, 205414. https://doi.org/10.1103/PHYSREVB.80.205414.

(109) Holmes, S. T.; Iuliucci, R. J.; Mueller, K. T.; Dybowski, C. Semi-Empirical Refinements of Crystal Structures Using 17O Quadrupolar-Coupling Tensors. *J Chem Phys* **2017**, *146*, 064201. https://doi.org/10.1063/1.4975170.

(110) Pickard, C. J.; Mauri, F. All-Electron Magnetic Response with Pseudopotentials: NMR Chemical Shifts. *Phys Rev B* **2001**, *63*, 245101. https://doi.org/10.1103/PhysRevB.63.245101.

(111) Adiga, S.; Aebi, D.; Bryce, D. L. EFGShield — A Program for Parsing and Summarizing the Results of Electric Field Gradient and Nuclear Magnetic Shielding Tensor Calculations. *Can J Chem* **2007**, *85*, 496–505. https://doi.org/10.1139/v07-069.

(112) Tumanova, N.; Tumanov, N.; Robeyns, K.; Fischer, F.; Fusaro, L.; Morelle, F.; Ban, V.; Hautier, G.; Filinchuk, Y.; Wouters, J.; Leyssens, T.; Emmerling, F. Opening Pandora's Box: Chirality, Polymorphism, and Stoichiometric Diversity in Flurbiprofen/Proline Cocrystals. *Cryst Growth Des* **2018**, *18*, 954–961. https://doi.org/doi.org/10.1021/acs.cgd.7b01436.

(113) Tumanova, N.; Tumanov, N.; Fischer, F.; Morelle, F.; Ban, V.; Robeyns, K.; Filinchuk, Y.; Wouters, J.; Emmerling, F.; Leyssens, T. Exploring Polymorphism and Stoichiometric Diversity in Naproxen/Proline Cocrystals. *CrystEngComm* **2018**, *20*, 7308–7321. https://doi.org/10.1039/C8CE01338A.

(114) Hasa, D.; Schneider Rauber, G.; Voinovich, D.; Jones, W. Cocrystal Formation through Mechanochemistry: From Neat and Liquid-Assisted Grinding to Polymer-Assisted Grinding. *Angewandte Chemie* **2015**, *127*, 7479–7483. https://doi.org/10.1002/ANGE.201501638.

(115) Lukin, S.; Germann, L. S.; Friščić, T.; Halasz, I. Toward Mechanistic Understanding of Mechanochemical Reactions Using Real-Time in Situ Monitoring. *Acc Chem Res* **2022**, *55*, 1262–1277. https://doi.org/10.1021/acs.accounts.2c00062.

(116) Gogoi, D.; Kalita, K. J.; Biswakarma, N.; Arhangelskis, M.; Deka, R. C.; Thakuria, R. Exploring Polymorphism, Stoichiometric Diversity and Simultaneous Existence of Salt and Cocrystal during Cocrystallization Using Mechanochemistry. *RSC Mechanochemistry* **2024**, *1*, 452–464. https://doi.org/10.1039/D3MR00022B.

(117) Hasa, D.; Carlino, E.; Jones, W. Polymer-Assisted Grinding, a Versatile Method for Polymorph Control of Cocrystallization. **2016**, *17*, 674–682. https://doi.org/10.1021/acs.cgd.6b00084.

View Article Online
DOI: 10.1039/D5MR00156K

(118) Ma, L.; Zheng, Q.; Unruh, D. K.; Hutchins, K. M. Reversible Interconversion of Pharmaceutical Salt Polymorphs Facilitated by Mechanical Methods. *Chemical Communications* **2023**, *59*, 7779–7782. https://doi.org/10.1039/D3CC02188B.

(119) Schmidt, R.; Martin Scholze, H.; Stolle, A. Temperature Progression in a Mixer Ball Mill. *International Journal of Industrial Chemistry* **2016**, *7*, 181–186. https://doi.org/https://doi.org/10.1007/s40090-016-0078-8.

(120) Gurau, G.; Kelley, S. P.; Di Bona, K. R.; Smiglak, M.; Rogers, R. D. Anhydrous Caffeine Hydrochloride and Its Hydration. *Cryst Growth Des* **2012**, *12*, 4658–4662. https://doi.org/10.1021/cg300878j.

(121) Peach, A. A.; Holmes, S. T.; MacGillivray, L. R.; Schurko, R. W. The Formation and Stability of Fluoxetine HCl Cocrystals Investigated by Multicomponent Milling. *CrystEngComm* **2023**, *25*, 213–224. https://doi.org/10.1039/D2CE01341J.

(122) Fischer, F.; Lubjuhn, D.; Greiser, S.; Rademann, K.; Emmerling, F. Supply and Demand in the Ball Mill: Competitive Cocrystal Reactions. *Cryst Growth Des* **2016**, *16*, 5843–5851. https://doi.org/10.1021/acs.cgd.6b00928.

(123) Jellinek, H. H. G.; Urwin, J. R. Ultraviolet Absorption Spectra and Dissociation Constants of Picolinic, Isonicotinic Acids and Their Amides. *Journal of Physical Chemistry* **1954**, *58*, 548–550. https://doi.org/10.1021/j150517a009.

(124) Day, G. M.; Chisholm, J.; Shan, N.; Motherwell, W. D. S.; Jones, W. An Assessment of Lattice Energy Minimization for the Prediction of Molecular Organic Crystal Structures. *Cryst Growth Des* **2004**, *4*, 1327–1340. https://doi.org/10.1021/cg0498148.

(125) Aitipamula, S.; Banerjee, R.; Bansal, A. K.; Biradha, K.; Cheney, M. L.; Choudhury, A. R.; Desiraju, G. R.; Dikundwar, A. G.; Dubey, R.; Duggirala, N.; Ghogale, P. P.; Ghosh, S.; Goswami, P. K.; Goud, N. R.; Jetti, R. R. K. R.; Karpinski, P.; Kaushik, P.; Kumar, D.; Kumar, V.; Moulton, B.; Mukherjee, A.; Mukherjee, G.; Myerson, A. S.; Puri, V.; Ramanan, A.; Rajamannar, T.; Reddy, C. M.; Rodriguez-Hornedo, N.; Rogers, R. D.; Row, T. N. G.; Sanphui, P.; Shan, N.; Shete, G.; Singh, A.; Sun, C. C.; Swift, J. A.; Thaimattam, R.; Thakur, T. S.; Kumar Thaper, R.; Thomas, S. P.; Tothadi, S.; Vangala, V. R.; Variankaval, N.; Vishweshwar, P.; Weyna, D. R.; Zaworotko, M. J. Polymorphs, Salts, and Cocrystals: What's in a Name? *Cryst Growth Des* **2012**, *12*, 2147–2152. https://doi.org/10.1021/cg3002948.

(126) Taylor, C. R.; Day, G. M. Evaluating the Energetic Driving Force for Cocrystal Formation. *Cryst Growth Des* **2018**, *18*, 892–904. https://doi.org/10.1021/acs.cgd.7b01375.

(127) Stone, J.; Edgar, J. O.; Rutherford, J.; Gill-Olivas, B.; Tranter, M.; Gould, J. A.; Xavier, C. M.; Telling, J.; Li, Y.; Wu, X.; Jiang, H. Flash Heating Boosts the Potential for Mechanochemical Energy Sources for Subglacial Ecosystems. *Frontiers in Geochemistry* **2023**, *1*, 1180893. https://doi.org/10.3389/FGEOC.2023.1180893.

(128) Michalchuk, A. A. L. On the Physical Processes of Mechanochemically Induced Transformations in Molecular Solids. *Chemical Communications* **2024**, *60*, 14750–14761. https://doi.org/10.1039/D4CC04062G.

View Article Online
DOI: 10.1039/D5MR00156K

(129) Ganduri, R.; Cherukuvada, S.; Sarkar, S.; Guru Row, T. N. Manifestation of Cocrystals and Eutectics among Structurally Related Molecules: Towards Understanding the Factors That Control Their Formation. *CrystEngComm* **2017**, *19*, 1123–1132. https://doi.org/10.1039/C6CE02003H.

(130) Beyer, M. K.; Clausen-Schaumann, H. Mechanochemistry: The Mechanical Activation of Covalent Bonds. *Chem Rev* **2005**, *105*, 2921–2948. https://doi.org/10.1021/cr030697h.

(131) Boldyreva, E. Mechanochemistry of Inorganic and Organic Systems: What Is Similar, What Is Different? *Chem Soc Rev* **2013**, *42*, 7719–7738. https://doi.org/10.1039/C3CS60052A.

(132) James, S. L.; Adams, C. J.; Bolm, C.; Braga, D.; Collier, P.; Frišcic, T.; Grepioni, F.; Harris, K. D. M.; Hyett, G.; Jones, W.; Krebs, A.; Mack, J.; Maini, L.; Orpen, A. G.; Parkin, I. P.; Shearouse, W. C.; Steed, J. W.; Waddell, D. C. Mechanochemistry: Opportunities for New and Cleaner Synthesis. *Chem Soc Rev* **2011**, *41*, 413–447. https://doi.org/10.1039/C1CS15171A.

(133) Gui, Y. Solid Form Screenings in Pharmaceutical Development: A Perspective on Current Practices. *Pharm Res* **2023**, *40*, 2347–2354. https://doi.org/10.1007/s11095-023-03573-2.

(134) Aaltonen, J.; Allesø, M.; Mirza, S.; Koradia, V.; Gordon, K. C.; Rantanen, J. Solid Form Screening – A Review. *European Journal of Pharmaceutics and Biopharmaceutics* **2009**, *71*, 23–37. https://doi.org/10.1016/J.EJPB.2008.07.014.

(135) Gowri, S.; Uma Devi, T.; Sajan, D.; Surendra Dilip, C.; Chandramohan, A.; Lawrence, N. Crystal Growth, Spectral, Optical and Thermal Properties of Semiorganic Nonlinear Optical Material: Picolinic Acid Hydrochloride. *Spectrochim Acta A Mol Biomol Spectrosc* **2013**, *110*, 28–35. https://doi.org/10.1016/J.SAA.2013.03.007.

(136) Bryce, D. L. Tensor Interplay. *eMagRes* **2008**. https://doi.org/10.1002/9780470034590.EMRSTM1039.

(137) Lacková, D.; Ondrejkovičová, I.; Padělková, Z.; Koman, M. Syntheses, Crystal Structures, and IR Spectra of Isonicotinamide-Isonicotinamidium Bis(Isonicotinamide)-Tetrakis(Isothiocyanato)Ferrate(III) and Isonicotinamidium Chloride. *J Coord Chem* **2014**, *67*, 1652–1663. https://doi.org/10.1080/00958972.2014.917634.

(138) Holmes, S. T.; Iuliucci, R. J.; Mueller, K. T.; Dybowski, C. Semi-Empirical Refinements of Crystal Structures Using 17O Quadrupolar-Coupling Tensors. *J Chem Phys* **2017**, *146*, 064201. https://doi.org/10.1063/1.4975170.

(139) Desiraju, G. R. Crystal Engineering: A Holistic View. *Angewandte Chemie International Edition* **2007**, *46*, 8342–8356. https://doi.org/10.1002/ANIE.200700534.

(140) Hirsh, D. A.; Holmes, S. T.; Chakravarty, P.; Peach, A. A.; DiPasquale, A. G.; Nagapudi, K.; Schurko, R. W. In Situ Characterization of Waters of Hydration in a Variable-Hydrate Active Pharmaceutical Ingredient Using 35 Cl Solid-State NMR and X-Ray Diffraction. *Cryst Growth Des* **2019**, *19*, 7349–7362. https://doi.org/10.1021/acs.cgd.9b01218.

(141) Hirsh, D. A.; Su, Y.; Nie, H.; Xu, W.; Stueber, D.; Variankaval, N.; Schurko, R. W. Quantifying Disproportionation in Pharmaceutical Formulations with 35 Cl Solid-State NMR. *Mol Pharm* **2018**, *15*, 4038–4048. https://doi.org/10.1021/acs.molpharmaceut.8b00470.

View Article Online
DOI: 10.1039/D5MR00156K

Table 1. Optimized conditions and ball milling parameters that lead to quantitative syntheses of each material.

Material	Type of HCl used (Solvent) [a]	Amount of HCl (Molar Equiv.)	Milling Time (Minutes)
NicH-Nic:H_2O	Aqueous	0.5	5
NicH	Aqueous	1	5
IsoH-Iso:H_2O [b,†]	Aqueous	0.5	2
IsoH [b]	Aqueous	1	2
PicH-Pic †	Aqueous	0.5	10
PicH:H_2O [c,†]	Aqueous	-	-
PicH †	Aqueous	1	5
NicAH	Aqueous	1	5
IsoAH	Aqueous	1	5
PicAH-PicA †	Aqueous	0.5	10
PicAH:H_2O	Aqueous	1	10
PicAH	Methanol	2	15
CaffH:H_2O	Aqueous	1	5
CaffH	Methanol	1	5
AcetH-Acet	Methanol	0.5	5
AcetH:H_2O	Aqueous	2	5
AcetH-Acet:H_2O †	Aqueous	1	5

[a] In instances where 12.1 M HCl(aq), 3.0 M HCl(MeOH), or 1.5 M HCl(EtOH) can be used, the 12.1 M HCl(aq) is preferred, due to the smaller volume of solvent.
[b] All LAG reactions used a milling frequency of 20 Hz, with the exception of those for **IsoH-Iso:H_2O** and **IsoH**, for which used a milling frequency of 30 Hz.
[c] Produced only via slow evaporation.
† Novel organic HCl salt, not previously reported.

View Article Online
DOI: 10.1039/D5MR00156K

Table 2. Results of competitive milling reactions involving two free bases and 12 M HCl(aq).[a]

Free Bases (1:1)	pK_a-1[b]	pK_a-2[b]	Amount of HCl (aq) (Molar Equivalents)	End Products[c]	Corresponding PXRD Figure in ESI
Nic + NicA	3.35	2.08	1	**NicH** + NicA	S8
Nic + NicA			0.5	**NicH-Nic:H_2O** + NicA	S8
Iso + IsoA[a]	3.61	1.70	1	**IsoH** + IsoA	S9
Iso + IsoA[a]			0.5	**IsoH-Iso:H_2O** + IsoA	S9
Pic + PicA	2.10	1.60	1	**PicAH-PicA + Pic-PicA**	S10
Pic + PicA			0.5	**PicAH-PicA** + **Pic-PicA**	S10
Nic + Iso	3.35	3.61	1	**IsoH-Iso:H_2O** + **Nic-Iso** + Nic	S11
Nic + Iso			0.5	**Nic-Iso**	S11
Nic + Pic	3.35	2.10	1	**NicH-Nic:H_2O** + **Nic-Pic**	S12
Nic + Pic			0.5	**Nic-Pic** + Pic	S12
Iso + Pic	3.61	2.10	1	**Iso-Pic:HCl** [e] + Pic	S13
Iso + Pic			0.5	**Iso-Pic:HCl** [e] + Pic	S13
NicA + IsoA	2.08	1.70	1	**NicAH** + IsoA + **IsoAH**[d]	S14
NicA + IsoA			0.5	**NicAH** + IsoA + NicA	S15
NicA + PicA	2.08	1.60	1	**NicAH** + **PicAH:H_2O** + NicA + PicA	S16
NicA + PicA			0.5	**PicAH:PicA** + NicA + **PicAH:H_2O**[d]	S17
IsoA + PicA	1.70	1.60	1	**PicAH:H_2O** + IsoA	S18
IsoA + PicA			0.5	**PicAH-PicA** + IsoA	S18

[a] All milling reactions were carried out with a milling rate of 35 Hz and milling time of 30 min, with the exception of Iso + IsoA reactions, which used 30 Hz and 60 min.
[b] pK_a-1 and pK_a-2 refer to the free bases on the left and right, respectively, in column 1.
[c] Reaction products are indicated in boldface.
[d] Minor phase, significantly less of this solid form is presen

Table 3. Comparison of reported and idealized mechanochemical conditions with literature routes for hydrochloride salt formation

	Mechanochemical Conditions Reported Herein						Idealized Mechanochemical Conditions [a]		Conditions Reported in Literature via Solution Methods			
Material	Mass of Free Base [b]	Chloride Source	Volume of Liquid [c]	Mass Produced [d]	PMI	Time (min)	Stoichiometric Liquid Required [c]	PMI	Chloride Source	PMI	Time (Days)	Ref #
NicH-Nic:H_2O	100.0	12.1 M HCl(aq)	34.0	112.9	1.15	2	33.8	1.15	Conc. HCl	8.4 [e]	14 [e]	70
NicH	75.0	12.1 M HCl(aq)	50.6	97.1	1.39	2	50.7	1.39	Conc. HCl	N/A	N/A	70
NicAH	75.0	12.1 M HCl(aq)	50.6	97.2	1.39	2	50.3	1.39	12 M HCl	100 [f]	N/A	9
CaffH:H_2O	75.0	12.1 M HCl(aq)	32.0	96.0	1.10	2	31.9	1.10	HCl(aq)	N/A	N/A	13
IsoH-Iso:H_2O	101.5	12.1 M HCl(aq)	35.0	124.1	1.15	2	34.3	1.15	N/A	N/A	N/A	N/A
IsoH	100.8	12.1 M HCl(aq)	70.0	130.9	1.41	2	68.2	1.39	12 M HCl(aq)	70	"Several"	10
PicH-Pic	202.8	12.1 M HCl(aq)	70.0	233.1	1.23	10	68.2	1.22	N/A	N/A	N/A	N/A
PicH	101.2	12.1 M HCl(aq)	70.0	131.4	1.40	5	68.5	1.39	N/A	N/A	N/A	N/A
IsoAH	101.4	12.1 M HCl(aq)	70.0	131.4	1.41	5	68.1	1.39	~0.6 M HCl(aq)	54 [f]	N/A	14
PicAH-PicA	101.6	12.1 M HCl(aq)	35.0	116.6	1.23	10	34.1	1.22	N/A	N/A	N/A	N/A
PicAH:H_2O	203.3	12.1 M HCl(aq)	140.0	293.3	1.26	10	136.5	1.25	Unknown [g]	N/A	N/A	15
PicAH	102.4	3.0 M HCl(MeOH)	550.0	132.7	4.63	15	277.3	2.71	HCl(aq) [h]	N/A	1	11
CaffH	101.7	3.0 M HCl(MeOH)	175.0	120.8	2.19	5	174.6	2.19	Acetyl Chloride / HCl(g)	30 (acetyl)	4	7
AcetH-Acet	103.3	3.0 M HCl(MeOH)	230.0	115.8	2.74	5	113.9	1.81	Acetyl Chloride	11	7	7
AcetH:H_2O	200.3	12.1 M HCl(aq)	220.0	272.5	1.70	5	109.5	1.21	Conc. HCl	7.3	30 min	120
AcetH-Acet:H_2O	202.5	12.1 M HCl(aq)	110.0	239.0	1.40	5	55.4	1.12	N/A	N/A	N/A	N/A

[a] Idealized mechanochemical conditions assume stoichiometric HCl addition enabled through optimization of milling parameters to maintain complete conversion without excess acid.
[b] Mass of free base is reported in g (above the solid black line) or mg (below the line).
[c] Volume of liquid is reported in mL (above the solid black line) or μL (below the line), for this work the density of 12.1 M HCl(aq) is assumed to be 1.19 g/mL, for HCl(MeOH) density is assumed to be 0.93 g/mL.
[d] Mass produced assumes 100% conversion of free base to respective HCl salt.
[e] PMI and time calculated only for crystallization step, preparation of NicH precursor not included (reported separately using excess conc. HCl).
[f] Estimated assuming 200 mg freebase, as substrate mass was not reported
[g] Most likely generated *in situ* from an Sb(III) chloride precursor (*e.g.*, $SbCl_3$, Ph_3SbCl_2, or Me_3SbCl_2)
[h] Inferred from aqueous hydrochloride crystallization conditions (exact synthesis not reported)

View Article Online
DOI: 10.1039/D5MR00156K

Table 4. ^{35}Cl EFG and chemical shift tensor parameters obtained from experimental measurements and DFT calculations on DFT-D2* geometry-optimized structures.

Material		$C_Q(^{35}Cl)$ [a] (MHz)	η_Q [a]	δ_{iso} [b] (ppm)	Ω [b] (ppm)	κ [b]	α [c] (°)	β [c] (°)	γ [c] (°)
NicH-Nic:H_2O	Exp	3.03(2)	0.83(2)	75.6(4)	70(10)	–0.8(2)	60(15)	85(10)	9(10)
	DFT	3.52	0.92	52	17	0.07	28	12	62
NicH	Exp	5.69(4)	0.12(2)	79.9(4)	75(10)	0.1(1)	40(10)	30(5)	120(10)
	DFT	–4.72	0.42	127.1	73	–0.02	230	39	165
IsoH-Iso:H_2O †	Exp	6.33(5)	0.81(4)	74(7)	40(15)	0.5 (4)	n/a [d]	15(15)	n/a [d]
IsoH	Exp	3.87(5)	0.83(2)	41.5(5)	57(10)	0.5(4)	40(10)	50(10)	125(15)
	DFT	3.72	0.58	65.4	81	–0.29	63	70	111
PicH-Pic †	Exp	1.24(3)	0.78(2)	63.1(5)	30(5)	–0.7(2)	65(20)	90(10)	90(10)
PicH:H_2O ‡	Exp	4.20(3)	0.74(2)	28.8(4)	160(20)	0.6(1)	0(10)	50(5)	20(10)
	DFT	4.29	0.99	49.7	121	–0.26	149	79	194
PicH †	Exp	2.25(2)	0.04(3)	25.5(4)	48(10)	–0.06(5)	90(10)	70(15)	90(30)
NicAH	Exp	7.26(3)	0.71(2)	60(7)	40(20)	0.5(4)	n/a [d]	n/a [d]	n/a [d]
	DFT	–6.21	0.58	60.7	130	–0.42	270	90	63
IsoAH (Site 1)	Exp	5.98(5)	0.74(3)	76(6)	81(20)	0.65(.35)	90(30)	45(5)	45(20)
	DFT	5.40	0.73	75.2	87	0.01	98	43	311
IsoAH (Site 2)	Exp	5.88(4)	0.57(3)	55(5)	65(15)	0.2(2)	45(20)	0(25)	124(25)
	DFT	5.83	0.54	43.2	57	0.30	104	76	212
PicAH-PicA †	Exp	4.94(3)	0.68(2)	35.1(4)	70(5)	-0.5(3)	0(15)	52(5)	27(10)
PicAH:H_2O	Exp	4.80(5)	0.81(3)	21.7(3)	110(10)	0.05(5)	0(10)	10(10)	90(10)
	DFT	5.24	0.85	57	137	–0.30	144	82	196
PicAH	Exp	9.52(6)	0.18(2)	28(10)	118(20)	–0.7(3)	n/a [d]	90(15)	90(15)
	DFT	–8.66	0.00	82.3	204	–0.45	180	90	276
CaffH:H_2O	Exp	5.22(4)	0.08(2)	11.1(4)	115(20)	–0.6	20(20)	67(10)	46(10)
	DFT	6.07	0.15	22.1	73	–0.55	288	85	186
CaffH	Exp	6.55(5)	0.40(2)	120(5)	10(10)	0(1)	n/a [d]	n/a [d]	n/a [d]
	DFT	–4.61	0.57	90.7	60	–0.62	359	22	94
AcetH-Acet	Exp	3.46(3)	0.13(2)	76.5(4)	40(10)	–0.5(3)	90(20)	90(20)	0(20)
	DFT	4.95	0.31	85.7	59	–0.46	302	83	355
AcetH:H_2O	Exp	3.37(3)	0.54(3)	56.2(4)	65(5)	–0.40(10)	100(10)	35(10)	90(20)
	DFT	4.08	0.60	60.6	59	–0.22	291	90	23
AcetH-Acet:H_2O†	Exp	1.59(2)	0.14(1)	58.9(4)	25(5)	0.5(2)	90(20)	25(5)	80(10)

[a] The principal components of the EFG tensors are defined such that $|V_{33}| \geq |V_{22}| \geq |V_{11}|$. The quadrupolar coupling constant and asymmetry parameter are given by $C_Q = eQV_{33}/h$, and $h_Q = (V_{11} - V_{22})/V_{33}$, respectively. The sign of C_Q cannot be determined from the experimental ^{35}Cl spectra. $Q(^{35}Cl)/Q(^{37}Cl) = -8.165/-6.435 = 1.27$.

[b] The principal components of the chemical shift tensors are defined using the frequency-ordered convention, with $d_{11} \geq d_{22} \geq d_{33}$. The isotropic chemical shift, span, and skew are given by $d_{iso} = (d_{11} + d_{22} + d_{33})/3$, $W = d_{11} - d_{33}$, and $k = 3(d_{22} - d_{iso})/W$, respectively.

[c] The Euler angles, a, b, and g, define the relative orientation of the EFG and chemical shift tensors using the *ZY′Z″* convention for rotation. The experimental angles derived from ssNake (which uses the *ZX′Z″* convention) are adjusted to match the calculated values extracted by EFGShield, which follows the *ZY′Z″* convention.

[d] This parameter is not reported since it has little effect on the appearance of simulated powder patterns.

† Novel organic HCl salt, not previously reported.

‡ Novel organic HCl salt, crystal structure reported herein.

View Article Online
DOI: 10.1039/D5MR00156K

Table 5. List of H···Cl⁻ contacts, associated moieties, and calculated ^{35}Cl SSNMR parameters for HCl salts, as determined from X-ray diffraction derived crystal structures.

Material	Number of short contacts	r(H···Cl⁻) of shortest contact (Å) [a]	r(H···Cl⁻) of 2nd shortest contact (Å) [a]	r(H···Cl⁻) of 3rd shortest contact (Å) [a]	r(H···Cl⁻) of 4th shortest contact (Å) [a]	Orientation of V_{33}	C_Q [b] (MHz)	η_Q [b]
NicH	1	2.063 RR′NH	2.217 RNH_2	-	-	Along/near the shortest H···Cl⁻ contact	–4.72	0.42
NicH-Nic:H_2O	0	2.206 H_2O	2.249 H_2O	2.290 RNH_2	-	Perpendicular to a plane of three hydrogen atoms	3.52	0.92
NicAH	1	1.962 RCOOH	-	-	-	Along/near the shortest H···Cl⁻ contact	–6.21	0.58
IsoH	2	2.164 RR′NH	2.197 RNH_2	-	-	Approx. perpendicular to H···Cl⁻···H plane	3.72	0.58
IsoAH (Site 1)	2	1.979 RCOOH	2.183 RR′NH	-	-	Approx. perpendicular to H···Cl⁻···H plane	5.40	0.73
IsoAH (Site 2)	2	1.987 RCOOH	2.120 RR′NH	-	-	Approx. perpendicular to H···Cl⁻···H plane	5.83	0.54
PicH:H_2O	2	2.170 H_2O	2.220 H_2O	2.250 RR′NH	-	Approx. perpendicular to H···Cl⁻···H plane	4.29	0.99
PicAH:H_2O	2	2.157 H_2O	2.180 H_2O	2.236 RR′NH	-	Approx. perpendicular to H···Cl⁻···H plane	5.24	0.85
PicAH	2	2.036 RCOOH	2.212 RR′NH	-	-	Along/near the shortest H···Cl⁻ contact	–8.66	0.00
AcetH:H_2O	3	2.120 ROH	2.183 H_2O	2.208 H_2O	2.313 RR′NH	Approx. perpendicular to H···Cl⁻···H plane	4.08	0.60
AcetH-Acet	2	2.067 ROH	2.251 RR′NH	2.285 RR′NH	-	Approx. perpendicular to H···Cl⁻···H planes	4.95	0.31
CaffH:H_2O	2	2.192 H_2O	2.195 H_2O	2.272 H_2O	2.337 H_2O	Along/near the shortest H···Cl⁻ contact [c]	6.07	0.15
CaffH	1	1.970 RR′NH	-	-	-	Perpendicular to the hydrogen bond [c]	–4.61	0.57

[a] H···Cl⁻ hydrogen bonds (r(H···Cl) ≤ 2.6 Å), as determined *via* energy minimization and geometry optimization with DFT plane wave calculations. Short H···Cl⁻ contacts are those with r(H···Cl) ≲ 2.2 Å.
[b] C_Q values and signs listed here are obtained from DFT calculations; the latter are unobtainable from $^{35/37}$Cl SSNMR experiments. It is noted that since $Q(^{35}Cl)$ = –8.165 fm², positive and negative values of C_Q correspond to negative and positive EFGs, respectively. Definitions of C_Q and η_Q are given in **Table 4**.
[c] Anomalous ^{35}Cl EFG tensor orientation, see discussion in text.

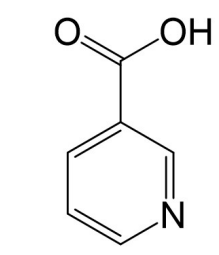

Nicotinic Acid (**NicA**)

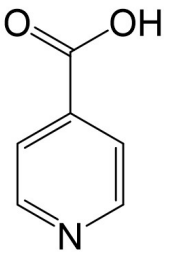

Isonicotinic Acid (**IsoA**)

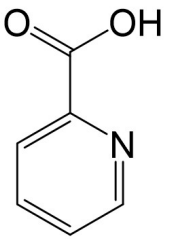

Picolinic Acid (**PicA**)

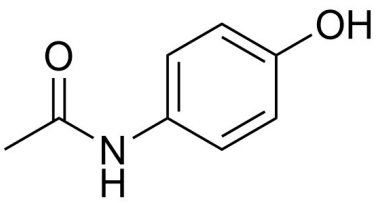

Acetaminophen (**Acet**)

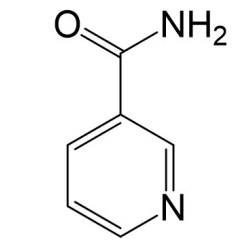

Nicotinamide (**Nic**)

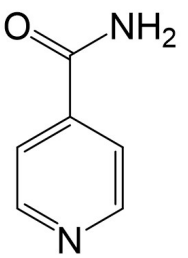

Isonicotinamide (**Iso**)

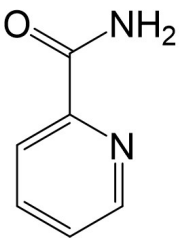

Picolinamide (**Pic**)

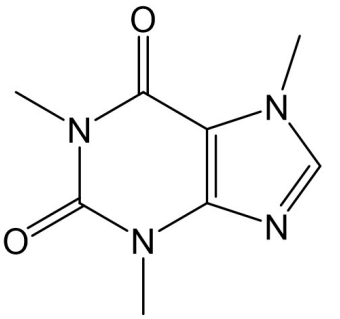

Caffeine (**Caff**)

Scheme 1. Free base molecules relevant to this work.

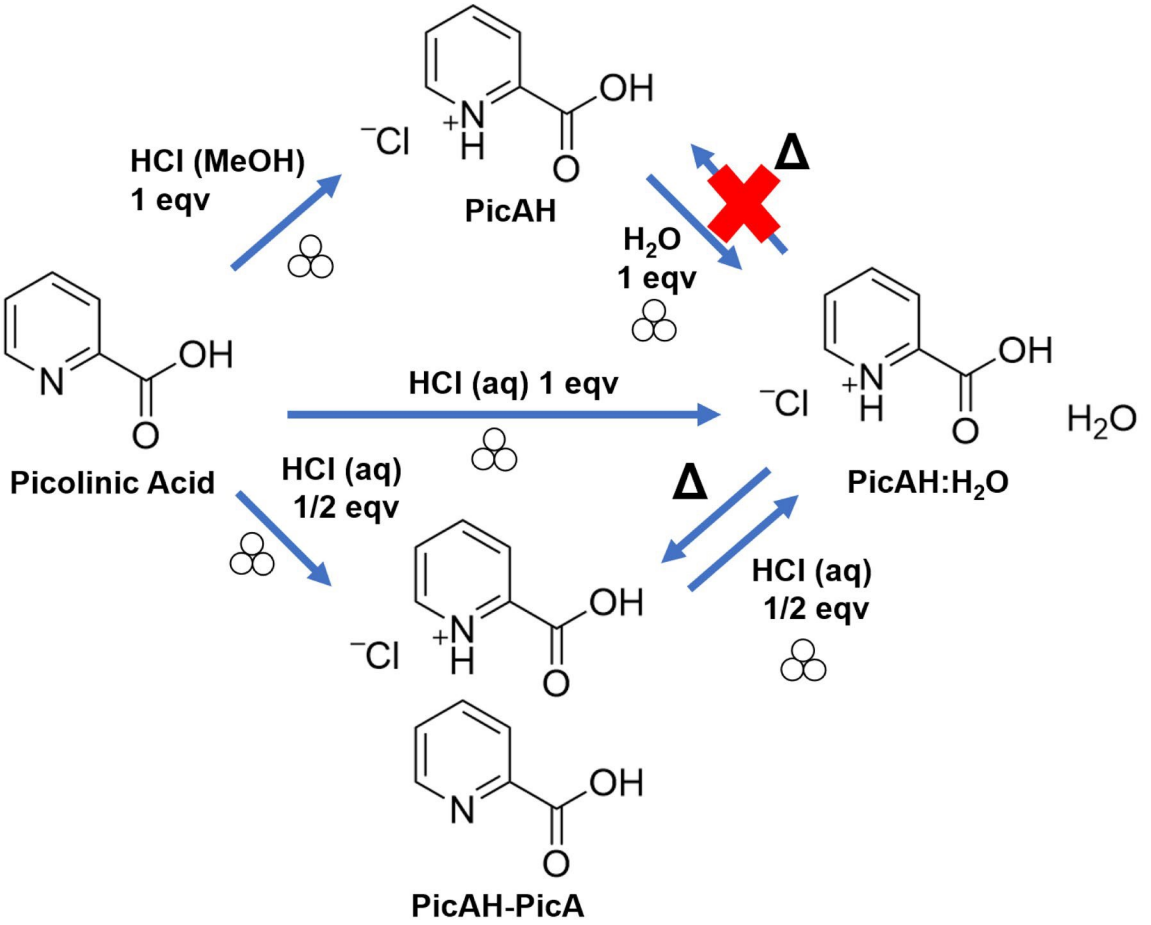

Fig. 1. Synthetic pathways for producing solid forms of picolinic acid (**PicA**), where, **PicAH** = picolinic acid hydrochloride, **PicAH:H_2O** = picolinic acid hydrochloride monohydrate, and **PicAH-PicA** = picolinic acid hemihydrochloride.

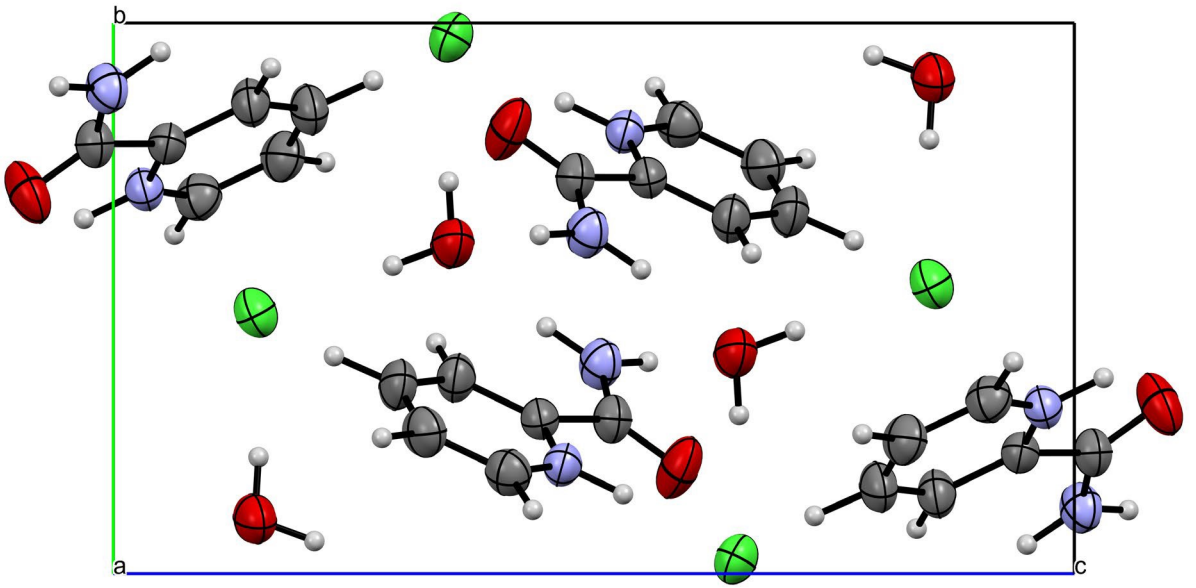

Fig. 2. ORTEP diagram of **PicH:H_2O** along the crystallographic *a*-axis.

View Article Online
DOI: 10.1039/D5MR00156K

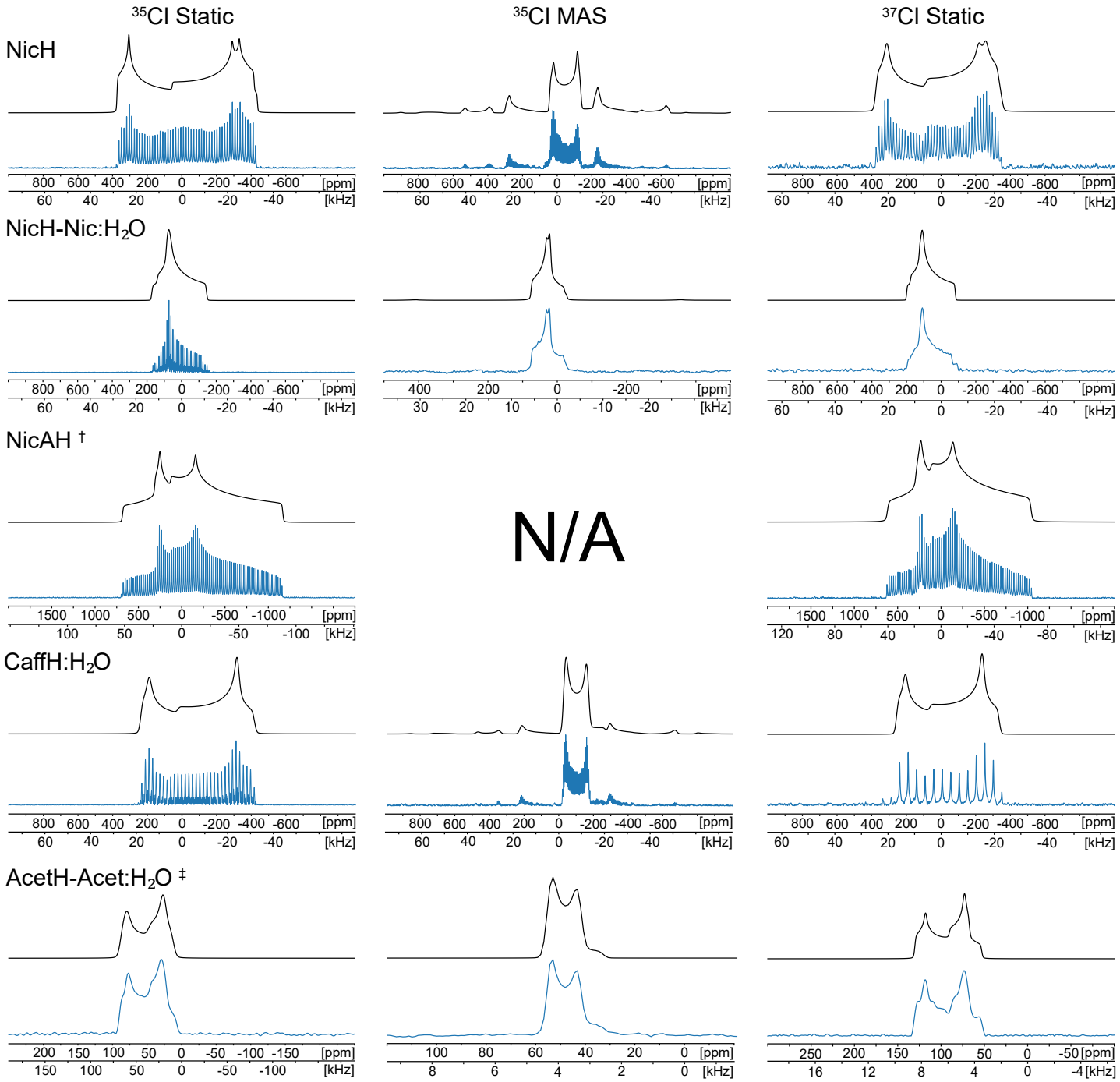

Fig. 3. Select $^{35/37}$Cl SSNMR spectra (blue) acquired at 18.8 T and corresponding simulations (black) of the CT powder patterns. † It is not possible to acquire an acceptable MAS pattern of this material using a 3.2 mm rotor at 18.8 T. ‡ **AcetH-Acet:H$_2$O** is the only salt in this subset without a known structure.

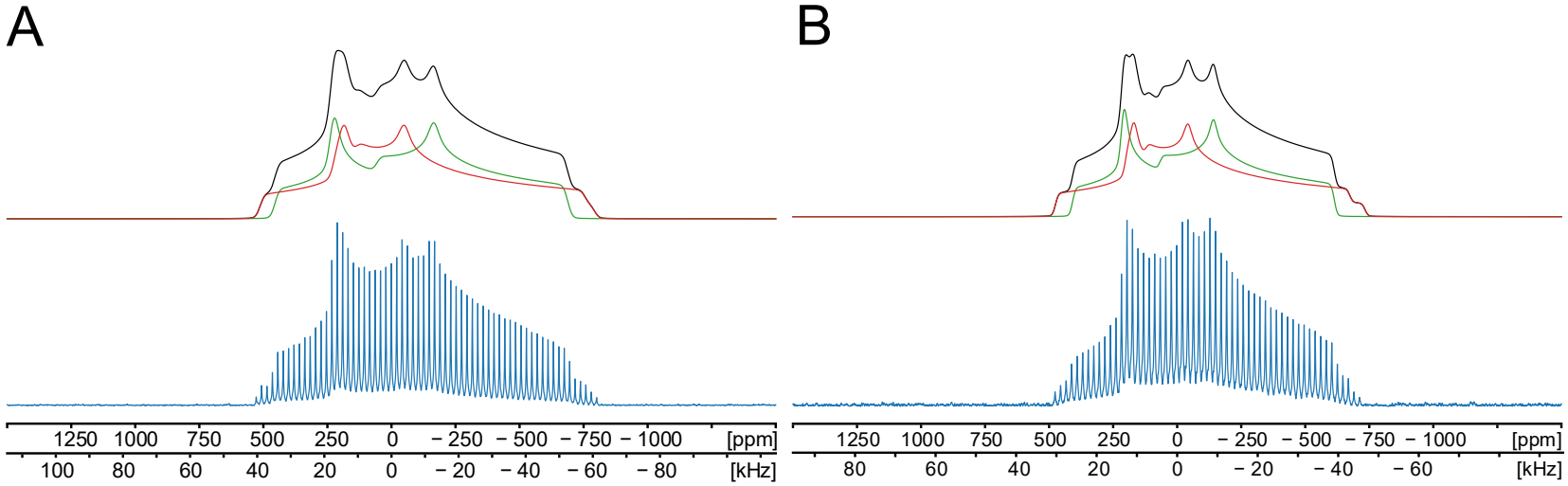

Fig. 4. (A) ^{35}Cl and **(B)** ^{37}Cl static SSNMR spectra of **IsoAH** acquired at 18.8 T, along with simulated patterns (black) and two-site deconvolutions (Site 1: red and Site 2: green).

View Article Online
DOI: 10.1039/D5MR00156K

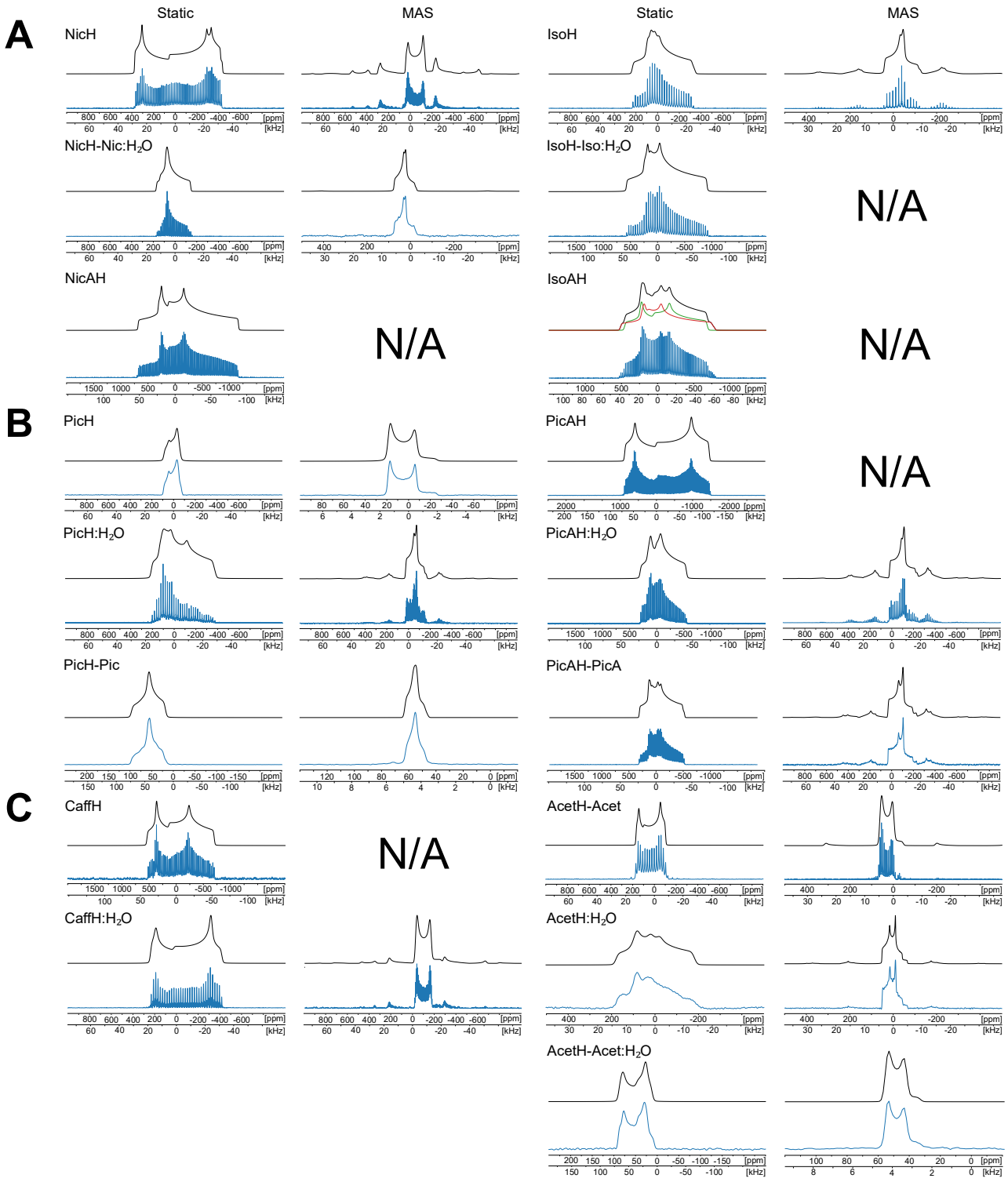

Fig. 5. ^{35}Cl static and MAS spectra (blue) and simulations (black, green, and red) of all synthesized HCl salts acquired at 18.8 T.

View Article Online
DOI: 10.1039/D5MR00156K

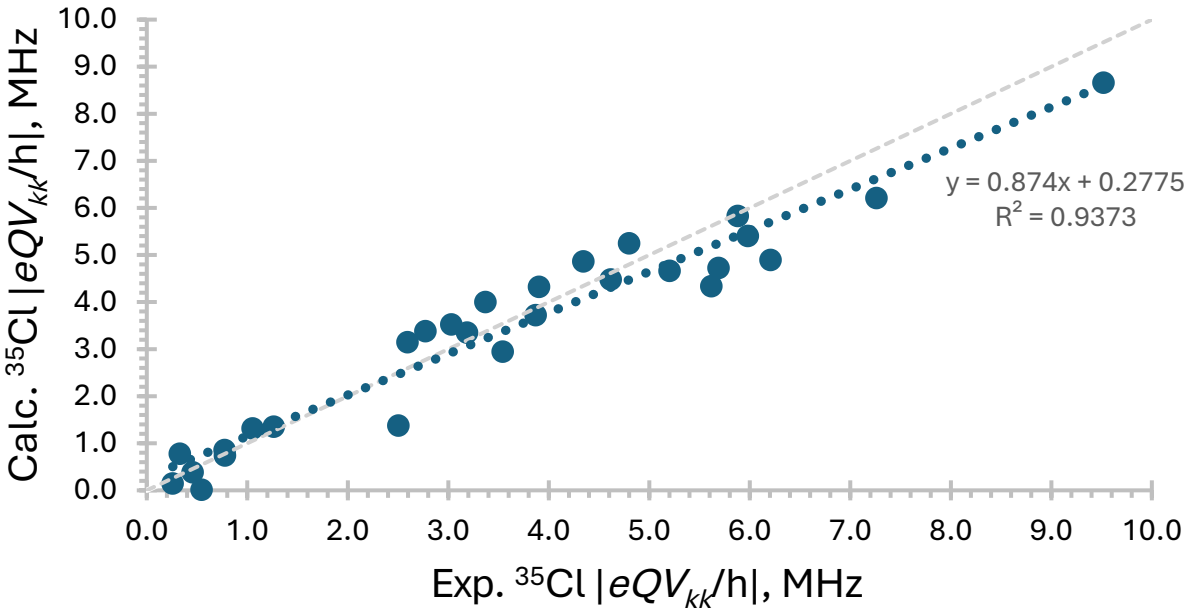

Fig. 6. Relationships between principal components of the ^{35}Cl EFG tensors that have been measured experimentally and calculated from DFT-D2* geometry optimized structures. The blue line represents the linear regression fit, while the grey line represents perfect correlation. **CaffH**, **CaffH:H_2O** and **AcetH-Acet** are excluded (see text for details).

View Article Online
DOI: 10.1039/D5MR00156K

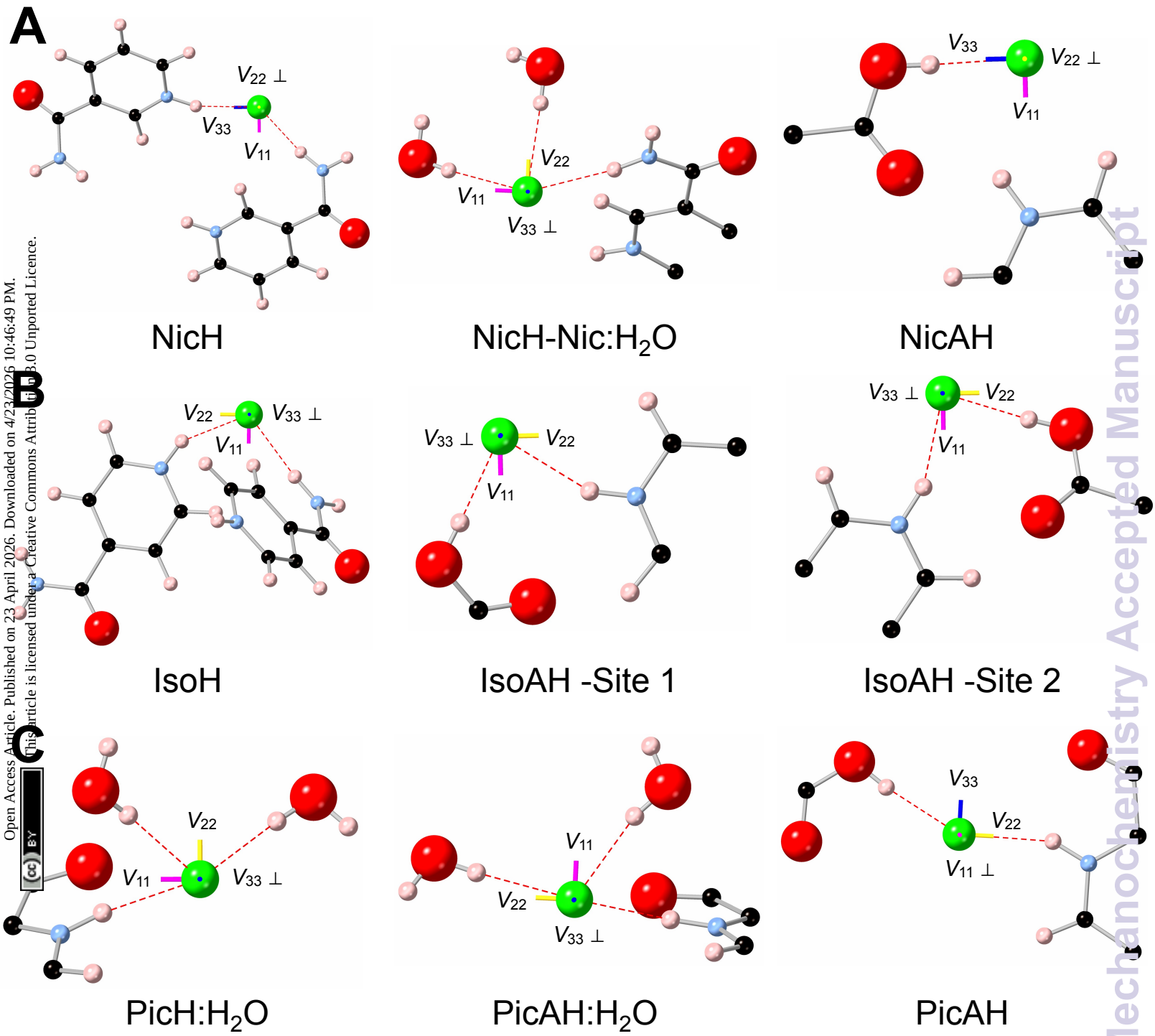

Fig. 7. ^{35}Cl EFG tensor orientations in: (A) **NicH**, **NicH-Nic:H_2O**, and **NicAH**; (B) **IsoH** and both chloride ions in **IsoAH**; and (C) **PicH:H_2O**, **PicAH:H_2O**, and **PicAH**. Red dotted lines indicate short contacts.

View Article Online
DOI: 10.1039/D5MR00156K

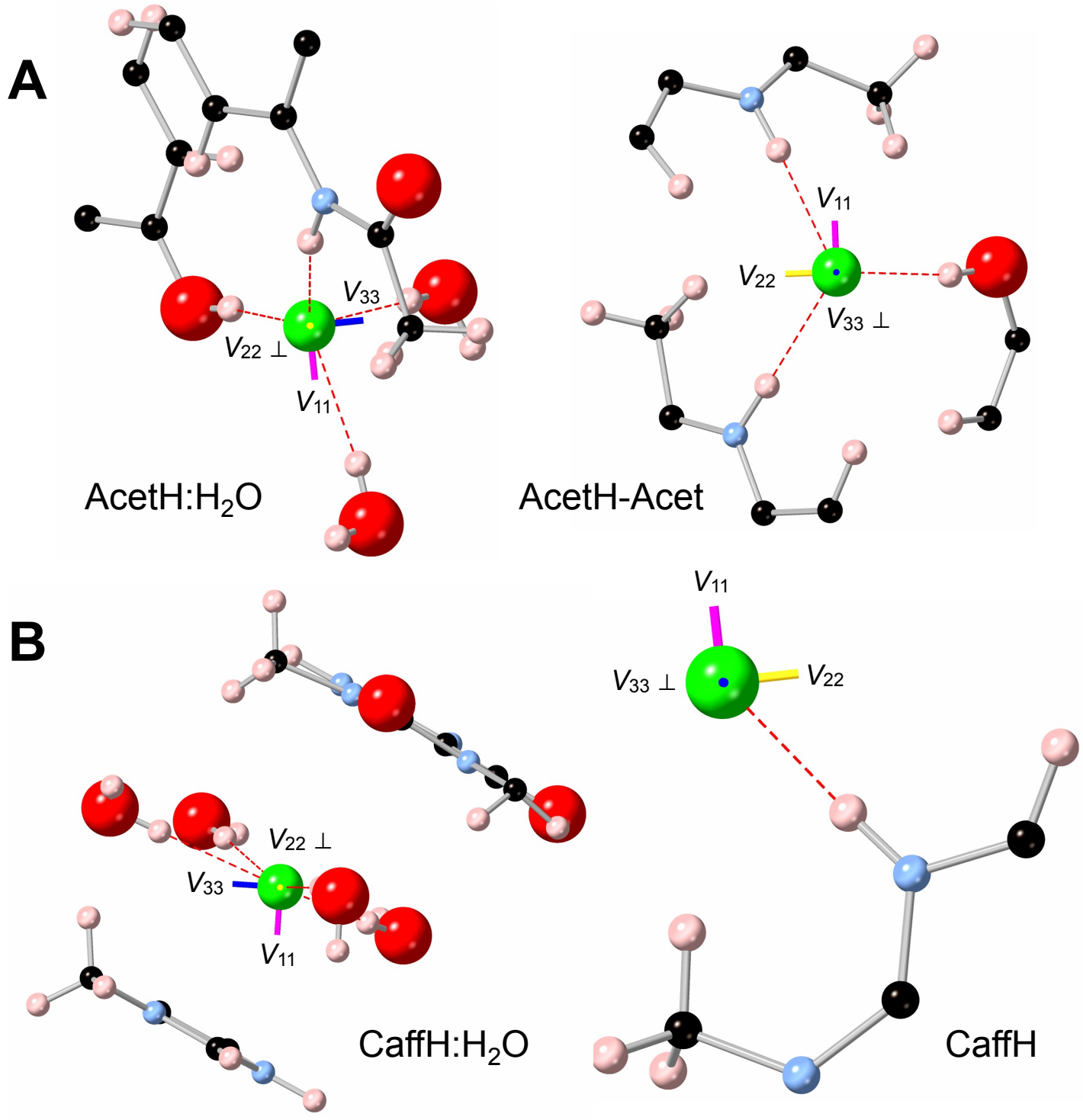

Fig. 8. ^{35}Cl EFG tensor orientations in: (A) **AcetH:H$_2$O**, and **AcetH-Acet**; and (B) **CaffH:H$_2$O**, and **CaffH**. Red dotted lines indicate short contacts.

View Article Online
DOI: 10.1039/D5MR00156K

Crystallographic data for picolinamide HCl monohydrate has been deposited at the CCDC under deposition number 2341820.